

The role of synaptic and voltage-gated currents in the control of Purkinje cell spiking: a modeling study

THE JOURNAL OF NEUROSCIENCE

(1997) 17:1: 91-106

Copyright © 1996 Society for Neuroscience

D. Jaeger¹, E. De Schutter², J.M. Bower¹

1. Div. of Biology 216-76, California Institute of Technology, Pasadena, CA 91125

2. Born Bunge Foundation, University of Antwerp - UIA, B2610 Antwerp, Belgium

Abstract

We have used a realistic computer model to examine interactions between synaptic and intrinsic voltage-gated currents during somatic spiking in cerebellar Purkinje cells. We have previously shown that this model generates realistic *in vivo* patterns of somatic spiking in the presence of continuous background excitatory and inhibitory input (De Schutter & Bower 1994b). In the present study we analyzed the flow of synaptic and intrinsic currents across the dendritic membrane and the interaction between the soma and dendrite underlying this spiking behavior. This analysis revealed that: 1) dendritic inward current flow was dominated by a non-inactivating P-type calcium current, resulting in a continuous level of depolarization; 2) the mean level of this depolarization was controlled by the mean rate of background excitatory and inhibitory synaptic input; 3) the synaptic control involved a voltage clamping mechanism exerted by changes of synaptic driving force at different membrane potentials; 4) the resulting total current through excitatory and inhibitory synapses was near-zero, with a small outward bias opposing the P-type calcium current; 5) overall, the dendrite acted as a variable current sink with respect to the soma, slowing down intrinsic inward currents in the soma; 6) the somato-dendritic current showed important phasic changes during each spike cycle; and 7) the precise timing of somatic spikes was the result of complex interactions between somatic and dendritic currents that did not directly reflect the timing of synaptic input. These modeling results suggest that Purkinje cells act quite differently from simple summation devices as has previously been assumed in most models of cerebellar function. Specific physiologically testable predictions are discussed.

The dendritic trees of single cerebellar Purkinje cells receive about 175,000 excitatory glutamatergic inputs from granule cells in the rat (Napper & Harvey 1988b), and about 1,500 GABA_A inputs from local interneurons (Korbo, Andersen, et al. 1993; Sultan, Ellisman, et al. 1995). Clearly, this

large number of inputs suggests that the synaptic control of somatic spiking in Purkinje cells could be quite complex. In addition, Purkinje cell dendrites are also known to have substantial dendritic voltage gated calcium currents and calcium-activated potassium currents (Llinás, Nicholson, et al. 1968; Llinás & Sugimori 1980b; Gruol, Dionne, et al. 1989; Usowicz, Sugimori, et al. 1992), which strongly influence membrane potential (Llinás & Sugimori 1980b; Llinás & Sugimori 1992), and can be activated by synaptic input (Eilers, Augustine, et al. 1995). One function of the activation of calcium currents with synaptic input may be the amplification of small synchronous synaptic inputs (De Schutter & Bower 1994c). It is still unclear, however, what pattern of current flow underlies the typical fast spontaneous spiking activity of 10 to 100 Hz of Purkinje cells recorded *in vivo* (Bower & Woolston 1983). Due to the large number of synaptic inputs it seems likely that Purkinje cells *in vivo* receive an ongoing baseline of synaptic activity. Such a pattern of many asynchronous synaptic inputs successfully reproduced the *in vivo* spike pattern in a realistic Purkinje cell model (De Schutter & Bower 1994b).

The objective of the present study was to use the realistic Purkinje cell model to examine the pattern of synaptic and voltage-gated dendritic currents that produces ongoing somatic spiking. We applied several new analysis techniques to examine this issue. We find that in the model intrinsic dendritic currents strongly influenced the time course of dendritic membrane potential. As a consequence, the timing of somatic spikes did not reflect the timing of particular synaptic inputs. The common assumption in cerebellar network models that Purkinje cell spiking reflects a simple summation of inputs (Marr 1969; Albus 1971; Fujita 1982; Kanerva 1988) may therefore not hold. Our predictions are readily testable through specific experiments. If experimentally confirmed, our modeling predictions have important consequences for theories of cerebellar function.

Materials and Methods

Model Construction

The model studied in this report is identical to the model previously described by De Schutter and Bower (1994a,b). The following sections will provide a brief overview of model construction and behavior. Readers interested in further details of model construction, parameter tuning, and comparison to established physiological data should consult the referenced papers.

Morphology and voltage-gated conductances.

The morphology of an HRP-injected Purkinje cell from a guinea pig cerebellum was reconstructed and a passive membrane model of the cell was made (Rapp, Segev, et al. 1994). Voltage-gated conductances were incorporated using known data about channel kinetics in the Purkinje cell when available (De Schutter & Bower 1994a). A total of 10 voltage-gated conductances were included in the model. Channel densities were then adjusted until the model replicated intracellular recordings of responses to somatic current injection (Llinás & Sugimori 1980a), including the

generation of dendritic calcium spikes and plateau potentials. The model best replicated these data when both the fast and persistent sodium conductance (NaF and NaP) were restricted to the soma and the high-threshold P-type calcium conductance (CaP) and two calcium activated potassium conductances (KC and K2) were restricted to the dendrite. Three other potassium conductances had mixed distributions, with the delayed rectifier (Kdr) and A-type K conductance (KA) mainly located in the soma but also found at a low concentration in the main dendrite close to the soma. A non-inactivating muscarinic type K conductance (KM) and a low-threshold calcium conductance (CaT) occurred at low densities both in the soma and in all dendritic compartments. A leak conductance with an amplitude determined by the input resistance of the cell was given a reversal potential of -80 mV, which provided for a stable resting membrane potential of the cell at -68 mV.

[Download the model scripts.](#)

Synaptic input.

After establishing the intrinsic conductances of the model, a set of synapses was added with the aim of replicating the expected natural input to the cell *in vivo* (De Schutter & Bower 1994b). Excitatory input from granule cells was simulated as synaptic conductances with an opening time constant of 0.5 ms, a closing time constant of 1.2 ms, a reversal potential of 0 mV, and a maximal conductance of 0.7 nS. These values match data of glutamatergic transmission via AMPA receptors (De Schutter & Bower 1994b; Stuart & Hausser 1994). One synaptic contact was made on each of 1,474 explicitly modeled spines that were attached to small-diameter dendrites. The reduced number of granule cell inputs in the model compared to real Purkinje cells (Harvey & Napper 1991) was compensated for by an increase in the frequency of activation of single synapses compared to physiological findings (Huang, Mu, et al. 1993). The validity of this tradeoff (Rapp, Yarom, et al. 1992) was confirmed by comparing results with a model including a larger number of synapses firing at a lower frequency. (De Schutter & Bower 1994b). Note, that even at the elevated granule cell input rate of 10 to 100 Hz used in the present study, little temporal overlap is to be expected between EPSPs of a single synapse due to the fast decay time constant. Stellate cell inhibition mediated by GABA_A receptors was simulated by synaptic conductances with a reversal potential of -80 mV, an opening time constant of 0.9 ms, and a closing time constant of 26.5 ms. These values were taken from a study on hippocampal pyramidal neurons (Ropert, Miles, et al. 1990). More recent recordings not available at the time of model construction indicated that the closing time constant of GABA_A receptors in the Purkinje cell is only in the range of 7-13 ms (Vincent, Armstrong, et al. 1992). To stay consistent with the previous modeling work we used our old time constants for GABA_A receptors, but added control simulations with the shorter decay time constant when a different outcome might be suspected. GABA_A synapses in the model had a peak conductance around 3 nS (varying with the size of the postsynaptic element) and were located directly on smooth and spiny dendritic compartments, resulting in a total of 1,695 such

contacts. Although the number of stellate cell inputs on a Purkinje cell has never been determined directly, it can be estimated from the ratio of stellate cells and Purkinje cells present in rat cerebellum (about 10:1, (Korbo, Andersen, et al. 1993) and the number of synapses a single stellate cell axon forms (about 150, (Sultan, Ellisman, et al. 1995) xxx). This estimation results in an average number of 1500 stellate cell inputs per Purkinje cell, which is close to the actual value used in our simulation studies.

The pattern of synaptic activation used here was identical to that used in our previous work (De Schutter & Bower 1994b). A random number generator was connected to all granule cell (gc) and stellate cell (sc) synapses. To simulate continuous baseline input, each synapse was activated individually with a random sequence of inputs. In any given simulation, the mean rate of these random inputs was identical for all gc synapses and a different mean rate was used to activate each sc synapse. Using input with this structure, we were able to approximate inter-spike interval distributions observed experimentally *in vivo* without making any changes to the model (De Schutter & Bower 1994b). This finding gives us confidence that the contribution of dendritic conductances to the behavior of the model was realistic.

Techniques for quantifying synaptic and voltage-gated currents

The primary objective of the present study was to examine the differential contribution of synaptic and voltage-gated conductances to dendritic depolarization and ultimately the spiking output of the modeled Purkinje cell. In order to do this, we have developed several new approaches to analyze the contribution of different conductances to the behavior of the model, as described below. In general, these techniques have allowed us to somewhat simplify the analysis of this very complex model.

Collapsing the spatial complexity of the dendritic tree: Total currents.

The principle form of simplification we have adopted to analyze the model involves collapsing the spatial distribution of dendritic membrane currents into total currents flowing across the entire dendritic surface. These total dendritic currents were calculated separately for each type of synaptic or voltage-gated current by adding the current from all dendritic compartments at each simulation time step. We have analyzed membrane currents rather than conductances as currents are directly related to the time course of membrane potential, which can be measured experimentally.

The contribution of individual conductances to membrane potential.

Most physiological experiments measure membrane potential over time. After having calculated the total current carried by each conductance we derived the contribution of individual conductances to membrane depolarization from the equation of a capacitor, $Q = C * V$ (Q is charge in Coulomb, C is capacitance in Farad, V is potential in Volt). As the dendritic capacitance of the Purkinje cell model is 4.2×10^{-9} F (1.64 mF / cm^2), a charge of 4.2×10^{-11} C is needed to depolarize the dendrite by 10 mV. This corresponds to a current of 0.42 nA flowing for 100 ms across the dendritic membrane. Each current flowing into the dendrite is either compensated by an opposing outward current, or contributes to membrane depolarization.

These relations allow us to attribute the time course of membrane potential to currents carried by individual types of conductances.

Interaction between the soma and the dendrite. In most mammalian neurons, the significance of dendritic current flow for neuronal processing ultimately lies in its effect on somatic spiking. In most Purkinje cells and in the model the only connection between the dendrite and the soma is provided by a single dendritic trunk. Using the model, we have analyzed the axial current flowing through this junction as it provides the only means of electrical information transfer between the soma and the dendrite. The amplitude of this somato-dendritic current (I_{s-d}) was calculated from the membrane potential of the soma (V_{ms}), the membrane potential of the initial dendritic segment (V_{mdi}) and the axial resistance between the two using Ohm's law as $I_{s-d} = (V_{mdi} - V_{ms}) / R_a$. Since the axial resistance between soma and the main dendrite is only 0.77 Meg Ω , even a small potential difference of 1 mV leads to a somato-dendritic current of 1.3 nA. The low capacitance of $4.6e^{-11}$ C of the soma entails that a current of 0.046 nA over 10 ms is sufficient to depolarize the soma by 10 mV.

Comparison of modeling results with experimental data

A critical test in the performance of a single cell model is its ability to replicate a whole range of physiological data. We have previously shown that the Purkinje cell model can replicate a wide range of intra- and extracellular data (De Schutter & Bower 1994a; De Schutter & Bower 1994b; De Schutter 1994). In the present analysis particular aspects of model behavior not previously demonstrated are also compared with physiological recordings, as described below.

Intracellular Purkinje cell responses to current injection

In order to analyze the role of voltage-gated conductances in the response to somatic current injection, we describe the detailed behavior of the model during and following a current injection pulse. The modeling results are compared with intracellular Purkinje cell recordings using matching current injection pulses. A detailed description of the *in vitro* guinea pig preparation used to acquire these data can be found in Jaeger and Bower (1994).

Inter-spike interval variability in neuronal spike trains

To compare the output spiking properties of the model with those of real Purkinje cells, extracellular spike data was obtained from crus IIa of rats under ketamine anesthesia. A detailed description of the preparation used to acquire these data can be found in Bower and Woolston (1983). Traces of spontaneous Purkinje cell spiking were used to construct inter-spike interval (ISI) distributions, which were then compared to a range of ISI distributions from the model derived from simulations with varying synaptic input conditions. Specifically, in several simulations we manipulated the variability of the synaptic input, ranging from constant gc and/or sc synaptic conductances to highly variable gc and/or sc inputs. Comparisons between the simulated and real ISI distributions allowed us to determine the likely effect of variability in synaptic input on spiking. In addition, we performed two analyses to tease apart the mechanisms by which input variability affects the timing between individual somatic spikes. First, we separated the

contribution of synaptic and voltage-gated dendritic membrane currents to fluctuations in dendritic membrane potential. Second, we constructed spike-triggered averages of V_{md} and each type of dendritic current for spikes divided into groups based on ISI duration. This allowed us to examine correlations between ISI duration and the time course of individual currents.

Results

Although the present paper is focused on understanding the interaction between synaptic currents and voltage-gated currents in the Purkinje cell, we will first examine the activation of voltage-gated currents with direct somatic current injection. As we will show, the activation of intrinsic currents with direct current injection bears many similarities to the case of synaptic input. It is easier, however, to support the modeling results with physiological data for the case of current injection than in the case of synaptic input, because the experimental conditions are much better controlled with current injection than with synaptic input.

Purkinje cell responses to current injection in vitro

As in many neurons, when current is injected into the soma of a Purkinje cell at resting membrane potential, a fast train of somatic action potentials is elicited (Fig. 1A; (Llinás & Sugimori 1980a)). In Purkinje cells, however, somatic spiking frequently continues beyond the duration of current injection (arrow in Fig. 1). We have previously shown that the Purkinje cell model used here replicates both aspects of Purkinje cell responses to current injection. (Fig. 1B; De Schutter and Bower, 1994a). Here we describe in more detail the intrinsic currents in the Purkinje cell model that form the basis for each aspect of this response.

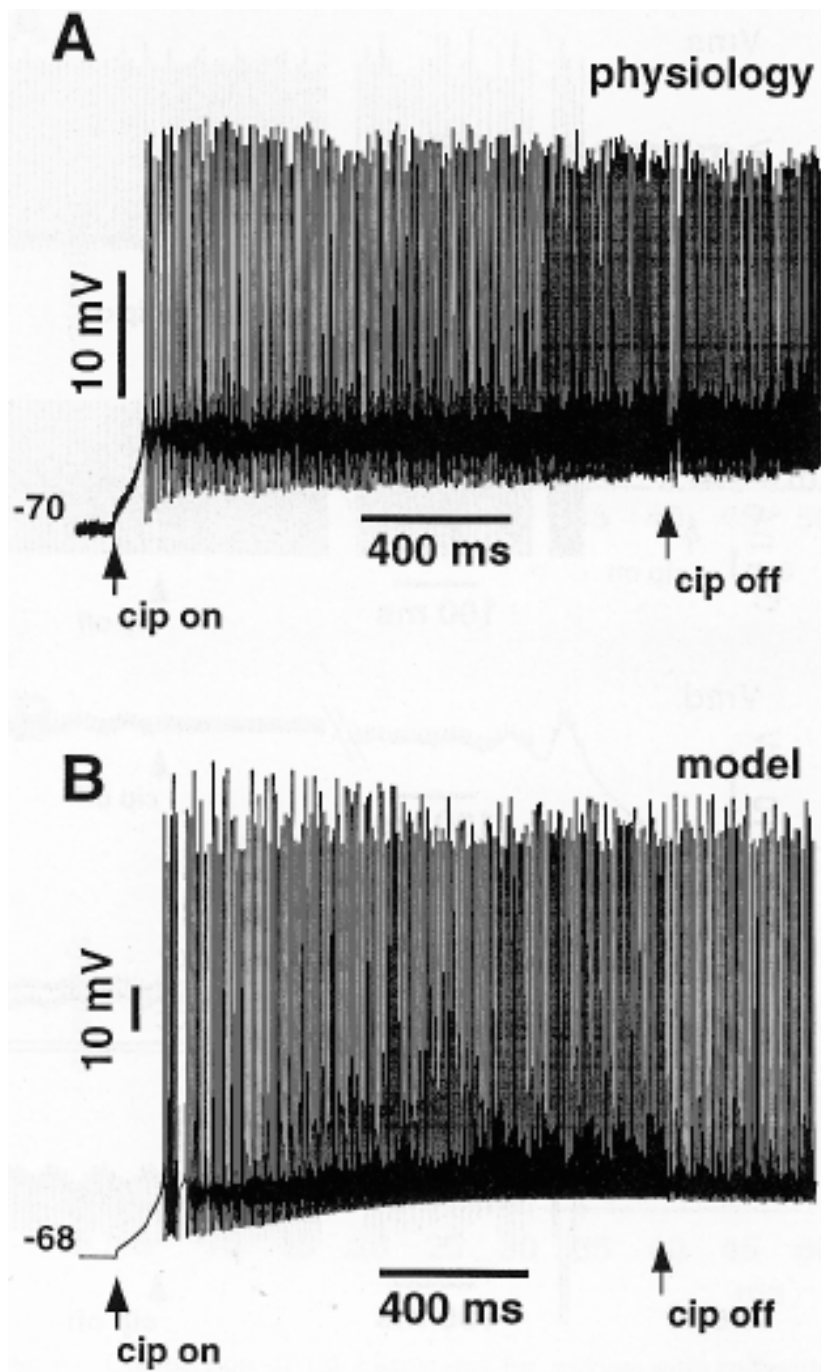


Figure 1

Comparison of voltage traces during current injection into the soma between a physiological recording and the model.

A: Intracellular recording of Purkinje cell soma *in vitro*. A current injection pulse (cip) of 1.5 s duration and 0.24 nA amplitude was started at 100 ms into the recording.

B: Somatic voltage trace of simulation of same current injection paradigm in the Purkinje cell model. In both cases, the current injection was started when the cell was in a quiescent state. The voltage response to current injection in the model and *in vitro* started with an initial period of slow depolarization, followed by fast regular somatic spiking followed. This spiking continued at a slightly reduced rate after offset of the current injection pulse (cip off).

Membrane currents during current injection.

Purkinje cells *in vitro* often remain silent for considerable periods of time. In the model, such stable resting potentials (-68 mV in Fig. 2A) were associated with a small amount of balanced inward and outward current (Fig. 2D,E). The onset of 0.24 nA current injection into the soma immediately led to an increasing depolarization of the soma. (Fig. 2A). Since the axial resistance between the soma and the main dendrite is low, 99% of the current injected into the soma passed directly into the dendrite, which also started depolarizing immediately (Fig. 2B).

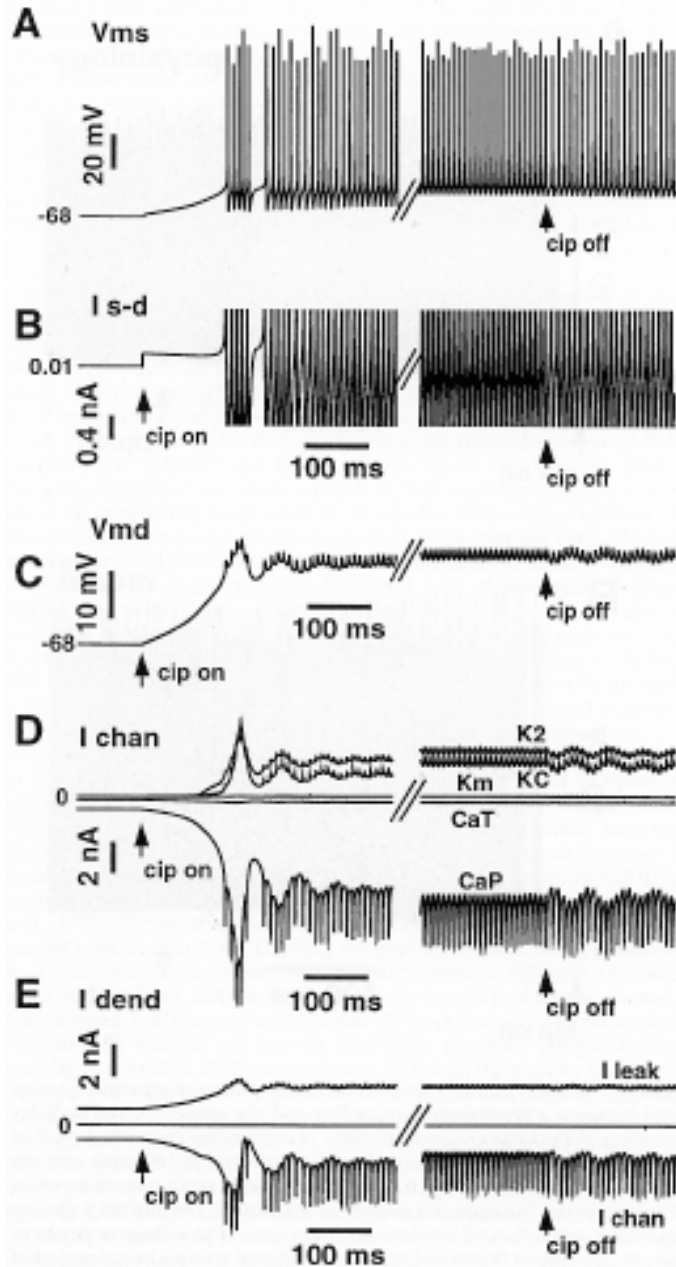


Figure 2

Current flow underlying voltage response to current injection in the model. Traces shown are taken from the same simulation for which the somatic voltage response is depicted in Fig. 1B. The time around onset and offset of the current injection pulse (cip) was expanded for improved resolution of details, and the middle section of current injection was left out.

A: Voltage response in the soma.

B: Current flow between the soma and the main dendritic segment. Current depolarizing the dendrite is depicted upward. The large amplitude of I s-d during somatic spiking (peaks at +25 and -2.2 nA) is truncated at ± 1.0 nA.

C: Dendritic membrane potential averaged over all dendritic compartments (V_{md}).

D: Dendritic currents through voltage-gated channels (I_{chan}) during the same simulation. The traces shown represent the summed current over all dendritic compartments for each conductance type. Inward (depolarizing) currents are depicted downward. See methods for description of each type of current.

E: The sum of all voltage-gated currents (I_{chan}) shown individually in (D) was largely compensated by the outward leak current (upper trace).

If all membrane conductances in the Purkinje cell model are blocked, we can calculate from the capacitance of the total membrane that the charge carried by the injected current of 0.24 nA would depolarize the whole cell within 280 ms to -52 mV (spike threshold in the active model). In the simulation with active conductances this value was reached both in the soma and in the mean dendritic potential in half this time (130 ms) (Fig. 2A,C), due to a net inward current with a mean amplitude of 0.54 nA. Accordingly, it is clear that the net current in the active model resulted from the sum of both injected and intrinsic currents. More detailed analysis of the model indicates that the most dominant inward current during this period was due to the activation of the dendritic CaP conductance, which had a mean amplitude of 1.74 nA (Fig. 2D). This inward current was balanced to a large degree by an outward leakage current with a mean of 1.48 nA and an outward dendritic K current with a mean of 0.26 nA (Fig. 2D,E). Note that these currents were much larger than the injected current itself. Therefore, the time course of membrane depolarization was mostly shaped by the active properties of the dendrite, especially by the CaP current. The role of the injected current is best understood as a 'command current', which had its largest effect on membrane potential by shifting the balance of dendritic voltage-gated currents.

Similar to the period of initial depolarization with current injection, the characteristics of the ensuing phase of sustained spiking were primarily governed by the balance of large intrinsic dendritic currents. In particular, the mean dendritic depolarization of -49.1 mV (Fig. 2C) was mostly sustained by a large inward P-type calcium current with a mean amplitude of 7.4 nA (Fig. 2D), with a much smaller contribution of 0.3 nA being made by the T-type calcium current. Inward currents into the dendrite were balanced by dendritic potassium currents with a mean amplitude of -5.4 nA (Fig. 2D), and the dendritic leak current of -2.65 nA (Fig. 2E).

As might be expected, during active spiking there was also a flow of current between the dendrite and the soma. Surprisingly, on average this current was from the soma to the dendrite, providing a mean flow of 0.45 nA to the dendrite (Fig. 2B). While the overall flow of current from the soma into the dendrite, the amplitude and direction of this current was strongly modulated during the time course of somatic action potentials. This phasic current flow was much larger than the injected current of 0.24 nA and determined the

time course of spiking. During the upswing of each action potential most of the large inward somatic NaF current flowed into the dendrite (Fig. 3). Since the dendrite has a high capacitance, however, this current led only to a small dendritic depolarization with each somatic spike (Fig. 2C). Subsequent activation of Kdr led to somatic spike after-hyperpolarization, and somatic Na currents were deactivated (Fig. 3). In contrast, the dendrite remained depolarized and a current with a peak amplitude of 2.5 nA flowed back into the soma from the dendrite (Fig. 3). Due to the small size and capacitance of the soma, this current effectively re-depolarized the soma following each spike. Overall, the interaction between soma and dendrite is best viewed as a dynamic push-and-pull operation, in which the soma mostly pushed current into the dendrite, but a phasic pull of current from the dendrite led to re-depolarization of the soma during spike after-hyperpolarization. This depolarization then reactivated the fast sodium current (NaF) in the soma, thus initiating an inward current flow across the somatic membrane. When the NaF current reached an amplitude of 0.5 nA, the somato-dendritic current reversed and again pushed current into the dendrite (second vertical dashed line in Fig. 3).

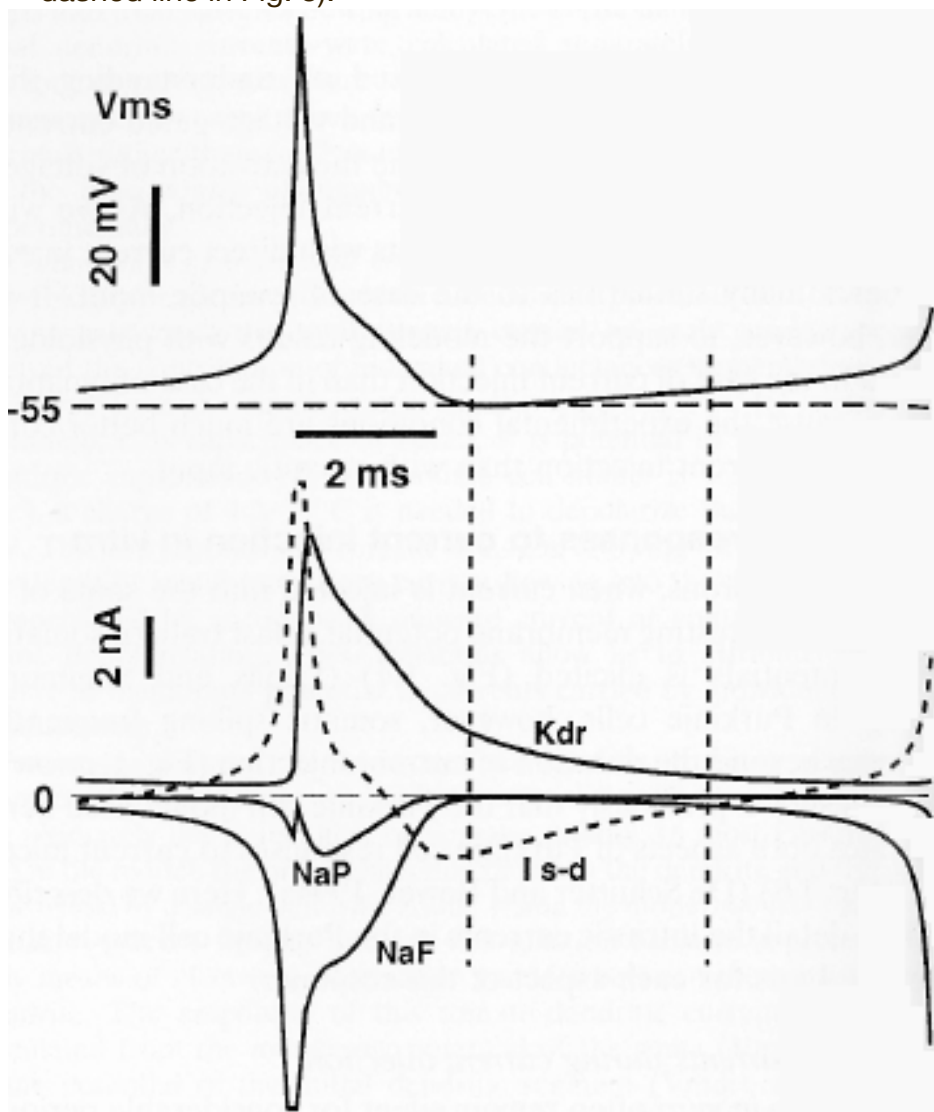


Figure 3

Somatic voltage and currents for a spike cycle after the offset of current injection. Somatic V_m (upper trace) and somatic currents (lower trace) during a spike cycle with current injection. Inward currents are plotted downwards. The dashed current trace represents the somato-dendritic current (I_{s-d}). The NaF and I_{s-d} currents are truncated at 10 nA maximal amplitude to give a better resolution of smaller currents. The first dashed vertical line marks the time of the most hyperpolarized somatic potential. Note that at this time I_{s-d} flowed into the soma with an amplitude of 2 nA due to maintained dendritic depolarization. The second dashed line marks the time in the spike cycle at which the injected current provided a significant proportion of the total inward current responsible for continued somatic depolarization.

Currents after the offset of current injection.

The activity of model conductances following the offset of current injection was surprisingly similar to the activity during the period of sustained spiking during current injection (Fig. 2). In fact, the mean level of dendritic depolarization changed only by 0.2 mV after the offset of current injection, and dendritic voltage-gated membrane currents showed only small changes (Fig. 2C-E). The continued depolarization was a result of the activation of inward P-type calcium conductance.

Analysis of the somato-dendritic current flow during somatic spiking after the offset of current injection showed the same pattern of current flow as during current injection. As described above, the dynamics of current flow during an action potential were governed by a dynamic push and pull operation between the soma and the dendrite (Fig. 3).

These findings show that the intrinsic properties of the Purkinje cell support fast regular spontaneous spiking at a depolarized membrane potential. In fact, the typical sequence of activity recorded *in vitro* leads to increasing depolarization during such spiking, and ultimately calcium spike bursting. We will now turn to the question how synaptic input may interact with these intrinsic properties.

Purkinje cell spiking in vivo.

In Figure 4 we contrast the pattern of spontaneous somatic spiking with spiking during continuous synaptic input for real and modeled data. The typical interspike-interval (ISI) distribution *in vitro* obtained just after the offset of current injection is very narrow, indicating very regular spiking (solid line in Fig. 4A). This narrow ISI distribution is quite similar to the pattern generated by the model following the offset of current injection (solid line in Fig. 4B). The typical ISI distribution for Purkinje cell spiking recorded *in vivo*, however, is quite different (dashed line in Fig. 4A). In particular, the *in vivo* data typically show a pronounced tail of long intervals and a higher degree of variability in spike intervals.

The Purkinje cell model was capable of generating ISIs similar to those seen *in vivo* when background excitatory and inhibitory synaptic activation was added (De Schutter and Bower, 1994b; dashed line in Fig. 4B). Given that ongoing spontaneous granule cell layer activity was recorded at the same time at which the Purkinje cell recordings from anesthetized rats shown in Fig. 4A were obtained (Jaeger and Bower, unpublished data), it seems reasonable to assume that Purkinje cells did receive a continuous

background of excitatory and inhibitory synaptic inputs in this situation. In the following sections we will examine the interplay of synaptic and intrinsic conductances underlying the spiking pattern of the model during a continuous background of synaptic inputs.

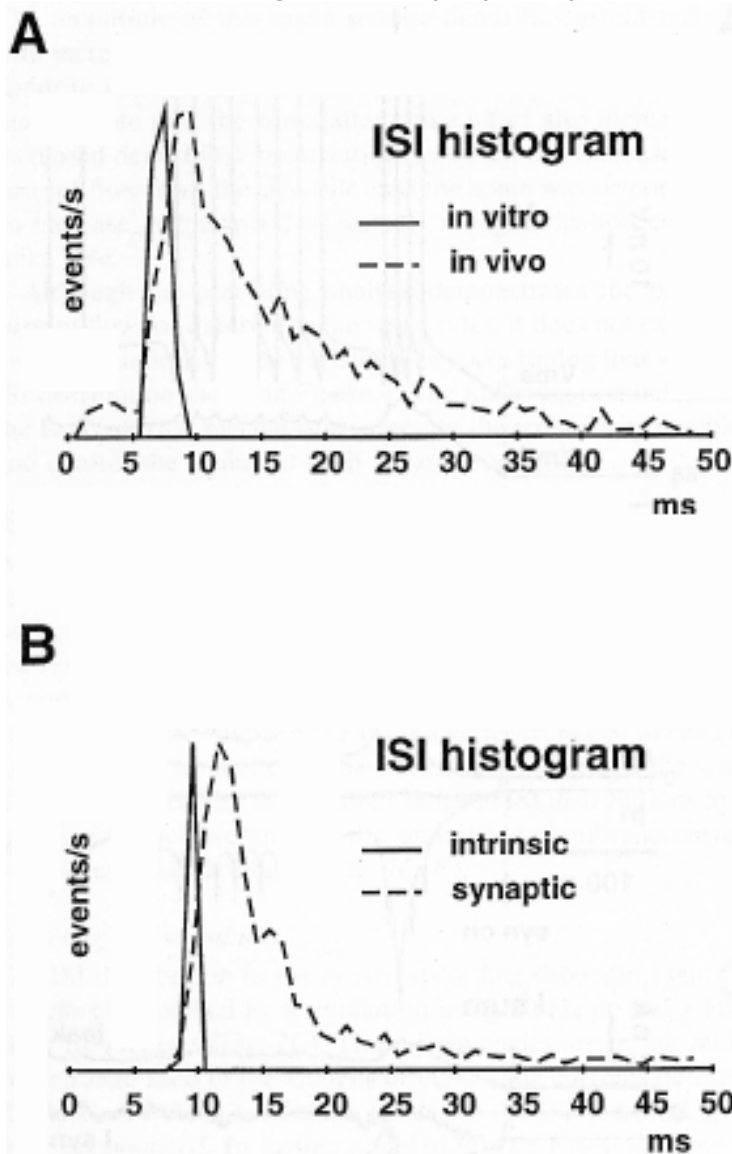


Figure 4

Comparison of interspike-interval histograms for spiking with and without synaptic input.

A: Physiological recording of extracellular activity *in vitro* (solid line) and *in vivo* (dashed line). The granule cell input is inactive under *in vitro* conditions, and inhibitory input through stellate cell inputs was blocked with bicuculline. Spontaneous spiking under these conditions most likely reflects purely intrinsic mechanisms. The resulting fast regular spike pattern showed a strong modal interval at 7.5 ms. The *in vivo* recording was obtained from an anesthetized rat in the absence of external stimulation. In this case the recorded cell is embedded in an intact cerebellar network and presumably receives a background of spontaneous synaptic inputs. The modal inter-spike interval of 9.5 ms was longer than in the *in vitro* case and a pronounced tail of very long intervals was present.

B: Spike-interval distributions obtained with the model in the absence (solid line) and presence (dashed line) of synaptic input. The spike train in the absence of synaptic input was obtained following a current injection of 0.24 nA. Synaptic input consisted of the random activation of all excitatory synapses at the rate of 37 Hz, and inhibitory synapses at 1.5 Hz. The obtained interval distributions closely resemble the physiological recordings under *in vitro* and *in vivo* conditions, respectively.

Response after the onset of synaptic input in the model

Figure 5 shows a simulation in which excitatory and inhibitory random background synaptic inputs were simultaneously initiated after 100 ms of simulation at the resting potential of -68 mV. The onset of synaptic input initiated dendritic depolarization in a ramp-like fashion at a rate of 3.2 mV every 10 ms (Fig. 5A). Depolarization of the soma was closely coupled to the dendrite, with a maximal difference between somatic potential and mean dendritic potential (V_{md}) of 0.4 mV. When somatic depolarization reached the spike threshold of -52 mV, the first somatic spike was triggered. A peak in V_{md} at 67 ms occurred after the onset of input and an associated brief burst of somatic spiking followed (Fig. 5A). At 100 ms after the onset of input V_{md} reached a plateau level with a mean of -52.2 mV (measured over 400 ms). At this level of dendritic depolarization the soma was activated to spike with a mean rate of 56 spikes per second (sps).

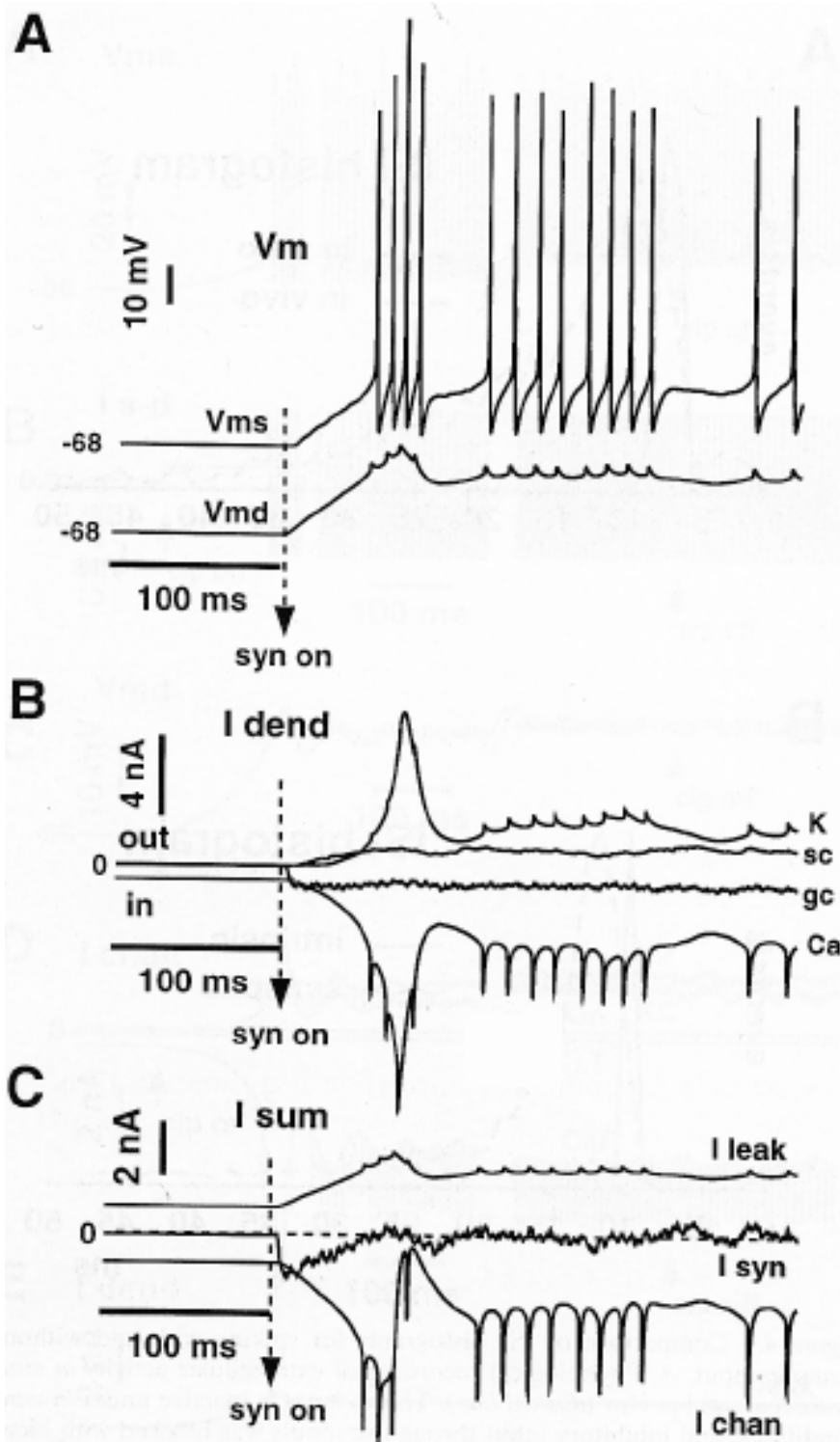


Figure 5

Voltage response and membrane currents resulting from asynchronous synaptic input. The simulation was started at the stable resting membrane potential (-68 mV), and after 100 ms synaptic input was turned on. Each gc synapse was activated randomly with a mean rate of 12 Hz, while each sc synapse was activated randomly with a mean rate of 0.5 Hz.

A: Membrane potential in the soma (Vms) and the average membrane potential over all dendritic compartments (Vmd).

B: Total dendritic currents summed over all compartments. All K currents were

combined (K trace) and the CaP and CaT current were also combined (Ca trace) in this and subsequent figures as both K currents with a significant amplitude (KC and K2) had the same pattern of activation and the CaT current did not contribute significantly to the total Ca current. The spikes in dendritic voltage-gated currents associated with somatic spikes were due to voltage transients conducted into the dendrite. Note that the spike triggered activation of the Ca current was larger than that of the K current, resulting in a net inward dendritic current flow for each somatic spike. Total synaptic currents are depicted in the traces marked as gc (excitatory) and sc (inhibitory).

C: The sum of inward and outward voltage-gated (I chan) and synaptic (I syn) currents is shown and contrasted with the leakage current out of the dendrite (I leak). While the summed synaptic current was close to zero, a net inward current was provided by the sum of voltage-gated currents. This inward current was counteracted by the leak current.

Synaptic and dendritic voltage-gated currents associated with synaptic input.

An important distinction between the direct current injection we examined above and the synaptic currents analyzed here lies in the fact that the amplitude of synaptic currents is dependent on the synaptic driving force, i.e. the distance of membrane potential from the synaptic reversal potential. For this reason, any change in membrane potential leads to an immediate change in driving force and hence of synaptic current.

When the synaptic input was turned on at the resting potential of -68 mV, the driving force for inhibitory input was low (-12 mV, reversal potential -80 mV), whereas the driving force for excitatory input was high (68 mV, reversal potential 0 mV). Consequently, the initial net synaptic current over the entire dendrite was dominated by excitatory input, reaching a peak amplitude of 1.5 nA at 6 ms after the input was turned on (Fig.5B,C). Due to the increasing dendritic depolarization following the onset of synaptic input, however, the driving force for excitatory input decreased whereas the driving force of inhibitory input greatly increased. As a consequence, the inward synaptic current decreased rapidly with increasing dendritic depolarization. In fact, when the dendritic membrane potential had reached its stable plateau with a mean of -52.2 mV (measured over 400 ms), the new balance in driving forces resulted in a total synaptic current that was now actually outward (i.e. inhibitory synaptic current) with a mean amplitude of -0.07 nA (Fig. 5C). Similar to the effect on intrinsic conductances of dendritic depolarization caused by somatic current injection, the initial depolarization caused by inward synaptic current activated a large P-type calcium current and at some delay a potassium current (Fig. 5B,C). Even before the total synaptic current decreased due to the change in driving forces described above, the amplitude of intrinsic inward current surpassed the amplitude of synaptic current and became the main cause for continued depolarization (Fig. 5B,C). Following a small peak in dendritic membrane potential caused by the delay between Ca and K current activation, the dendrite was kept depolarized at its plateau level due to a balance of inward and outward currents very similar to the current levels seen with somatic current injection. This balance consisted of a mean Ca current of 5.8 nA, a mean K current of -3.1 nA, and a mean leak

current of -2.4 nA.

The control of dendritic depolarization by synaptic conductances.

As described above, the mean synaptic current was close to zero in the dendritic plateau depolarization associated with continuous synaptic input (Fig. 5C). Nevertheless, the synaptic input still controlled the overall level of depolarization as any change in potential resulted in a change in driving forces of synaptic currents that led to a 'control' current bringing the overall balance back to its stable point. This mechanism by which a baseline of open synaptic conductances stabilizes dendritic V_m can be described as a partial voltage-clamp (Staub, De Schutter, et al. 1994) because any deviation in voltage is counteracted by an opposing change in synaptic current. The exact clamping voltage for steady state conductances is given by $V_{\text{clamp}} = g_{\text{ex}}V_{\text{ex}} + g_{\text{in}}V_{\text{in}} / (g_{\text{ex}} + g_{\text{in}})$, where $g_{\text{ex/in}}$ and $V_{\text{ex/in}}$ are the excitatory and inhibitory conductances and reversal potentials, respectively. For example, V_{clamp} in the model for the mean conductances associated with at a rate of 1.5 Hz inhibition and 33 Hz excitation (output spike rate 12 sps) comes to -56.6 mV. A second important number here is the clamping gain, i.e. the amount of synaptic current induced per mV of deviation from V_{clamp} . This gain (Gn_{clamp}) is given by $Gn_{\text{clamp}} = (g_{\text{ex}} + g_{\text{in}}) * 1 \text{ mV}$. For 1.5 Hz inhibition, 33 Hz excitation Gn_{clamp} comes to 0.25 nA in the model. This clamping effect of synaptic conductances exerted a controlling force on the dendritic membrane potential, and without time delay counteracted any intrinsic currents that tended to break away from V_{clamp} .

Somato-dendritic current during spiking with synaptic input.

The pattern of current flow between dendrite and soma during each spike cycle was identical to the case with current injection described above (Fig. 3). That is, during spike after-hyperpolarization a current flowed back from the dendrite into the soma. This current was necessary to re-depolarize the soma and its amplitude was controlled by the level of dendritic depolarization. Current flow was from the soma into the dendrite, however, following spike after-hyperpolarization and during spikes. As a result, the mean current between soma and dendrite over 400 ms of spiking was outward into the dendrite with an amplitude of 0.17 nA. Thus, even when somatic spiking was controlled by dendritic synaptic input, the dendrite acted overall as a current sink with respect to the soma.

Quantitative evaluation of currents for different levels of synaptic input.

The above analysis was carried out using a constant background frequency of excitatory and inhibitory inputs, which produced a spike rate of 56 sps. Purkinje cells recorded *in vivo* show maintained spike rates in the range of 10 - 140 sps (Bower & Woolston 1983). We have previously shown that the model is capable of generating this whole range of spike rates with appropriate levels in background synaptic input (De Schutter & Bower 1994b). Further, the previous study demonstrated that the same spike rate could result from different levels of input, if an increase in inhibition was matched by an increase in excitation. In general, the rate in spiking remained the same when the rate of excitatory input was increased by 15 Hz for every

increase of 0.5 Hz in sc input (Fig. 6A; also De Schutter and Bower, 1994b, Fig. 9A). Here we analyze the currents responsible for this behavior for a range of gc input from 10 to 100 Hz and sc input from 0.5 to 2.0 Hz (Fig. 6B-E).

When different levels of excitatory and inhibitory input frequencies produced the same spike rate, the concomitant levels of somatic and dendritic membrane potential (Fig. 6B) were virtually identical. Any increase in spiking rate was associated with an increase in the mean level of somatic and dendritic depolarization (Fig. 6B). Over the entire range of physiological spike rates between 10 and 140 sps the soma was on average more depolarized than the dendrite (Fig. 6B), meaning that the dendrite overall acted as a current sink at all somatic spike rates.

Somewhat surprisingly for all combinations of gc and sc input rates producing spike rates between 10 and 120 sps the mean synaptic current over the entire dendrite was close to zero, with a small outward bias (Fig. 6D). Maintained dendritic depolarization with a net synaptic outward current was possible as inward voltage-gated currents balanced the sum of outward dendritic currents (total synaptic current, potassium and leak current) at membrane potentials supporting physiological spike rates (Fig. 6C). Even though the synaptic current was close to zero, the level of open synaptic conductances controlled dendritic depolarization through the partial voltage clamping mechanism described above. In fact, the small size of synaptic current indicates that dendritic membrane potential was close to the clamping potential given by the baseline level of open synaptic conductances with different rates of input. To achieve spike rates greater than 120 Hz, however, an increasing net inward synaptic current was necessary (Fig. 6D). This increase in inward synaptic current was needed because at the more depolarized membrane potential supporting such high spike rates the balance between dendritic Ca and K currents shifted toward a net outward current (Fig. 6C). As a result, the dendrite was less depolarized than predicted from the synaptic clamping potential.

The mean somato-dendritic current was outward into the dendrite for the entire range of input frequencies tested (Fig. 6E). The amplitude of this mean somato-dendritic current increased with increasing spike rate due to the charge injected into the dendrite with each spike. Nevertheless, the phasic current from the dendrite into the soma following spike offset also increased with increased dendritic depolarization. In effect, this increased phasic current flow from the dendrite into the soma was responsible for an increase in the speed of somatic re-depolarization and hence spike rate.

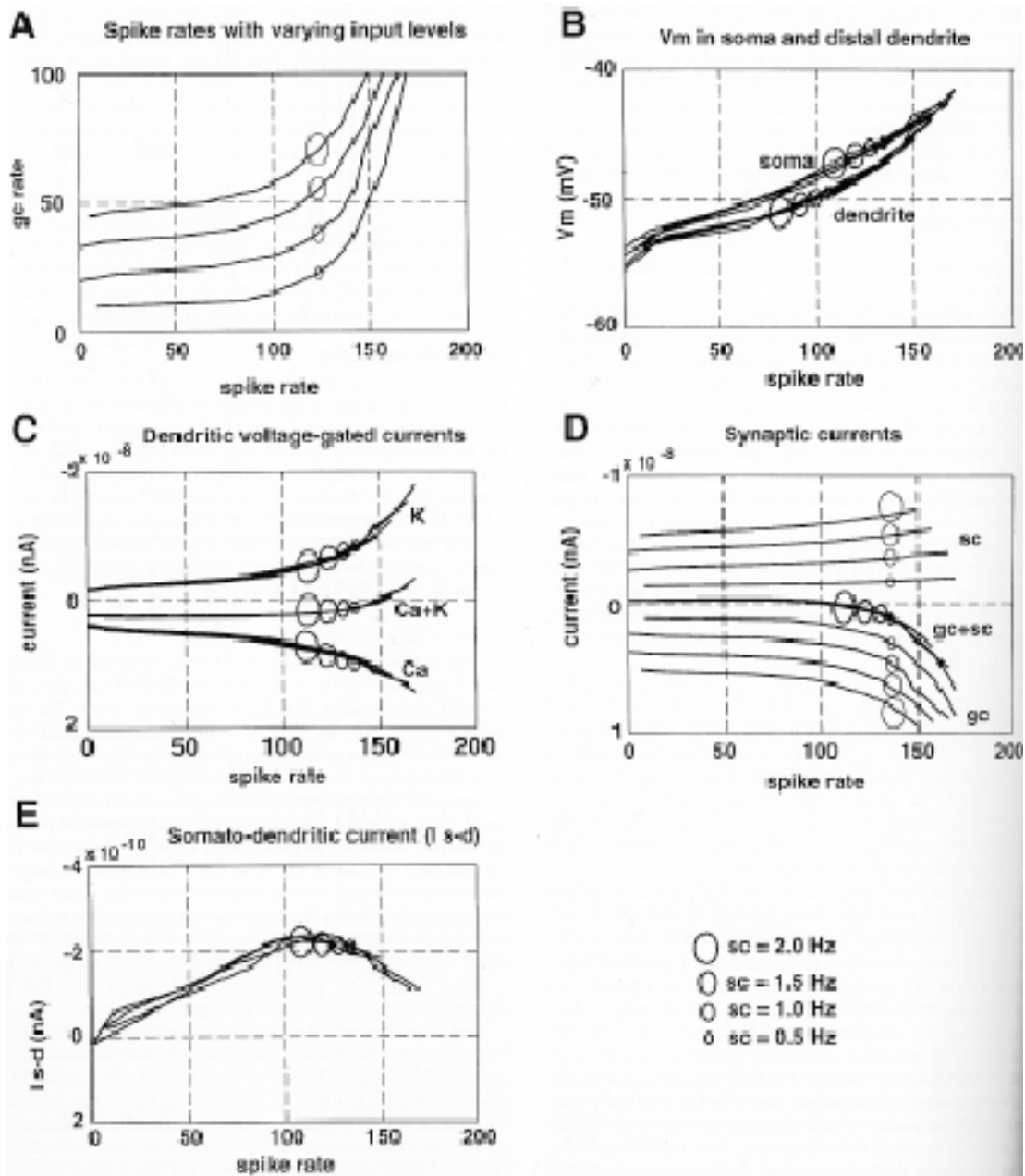


Figure 6

Summary diagram of current amplitudes associated with various levels of gc and sc input. Simulations were run for a period of 2.0 s for each level of synaptic input. The first 1.5 s were treated as equilibration period and only the final 0.5 s were analyzed for spike rates and current amplitudes. In each panel of the figure, different levels of sc inhibition (0.5, 1.0, 1.5, 2.0 Hz) are depicted as separate curves. For each curve, the gc input rate was increased in small steps to study voltage responses and current amplitudes.

A: Somatic spike rate as function of gc and sc input frequency. Note that the same spike rate could result from different total levels in synaptic input.

B: Average membrane potential in soma and dendrite for different spike rates. Note that the soma was on average more depolarized than the dendrite and that the difference in potential is roughly proportional to the somato-dendritic current (E).

C: Dendritic voltage-gated currents. Inward current (combined Ca currents) is down,

outward current (combined K currents) is up. The sum of inward and outward currents (Ca + K) is inward for spike rates up to 150 sps. The leak current counteracting this current to produce a stable membrane potential is not shown. Currents for the 4 different levels of inhibition are superimposed.

D: Total inward (gc) and outward (sc) synaptic current as function of somatic spike rate. Inward current is down. The sum of inward and outward synaptic current (gc + sc) was outward for spike rates up to 120 sps. The summed traces for different level of inhibition lie on top of each other.

E: Temporal average of current flowing between soma and dendrite (I s-d). While this current was strongly modulated during each spike cycle (Fig. 3), the mean direction of flow from soma to dendrite does indicate that overall the soma acted as a current source rather than as a current sink.

While the preceding analysis demonstrates the pattern of current flow for different mean spike rates, it does not explain the processes underlying the variability in spike timing that shape the ISI distribution shown in Fig. 4. The following sections address the issue of what mechanisms generate the irregularity in spiking and control the timing of each spike in the model.

Interspike-interval variability in vivo

As we have already described, *in vivo* spike trains from Purkinje cells and spike trains in the model produced in the presence of background synaptic input typically show a pronounced mode in the ISI distribution around 10 ms and a tail of long ISIs (Fig. 4). A comparison between different Purkinje cells recorded *in vivo* indicates that the shape of the ISI tail varies from cell to cell (Fig. 7A,B). Below, we first examine what characteristics of the synaptic input may account for a similar range in ISI distributions in the model, and then we analyze the underlying membrane currents producing spike variability (Fig. 7C-F).

Source of ISI variability.

The ISI distribution in the *in vivo* recording shown in Fig. 7A was closely matched by a simulation using 30 Hz gc and 1 Hz sc input frequencies (Fig. 7C). These frequencies are in the middle of the range used in the analysis of membrane currents described above. Under these conditions the tail in the ISI distribution was quite pronounced. In further simulations we examined how the observed ISI distribution depended on variability of the synaptic input. First, we tested whether spike variability could be produced without any variability in the synaptic input. To do this, we partly opened each synapse in the model at a constant level, such that the constant synaptic conductance matched the mean synaptic conductance level with 30 Hz gc and 1 Hz sc input. As output the model produced regularly spaced spikes with an ISI of 14.5 ms, which was close to the modal interval seen with 30 Hz gc and 1 Hz sc input. This result indicates that the tail of long ISIs is a consequence of fluctuations in the input.

Next we compared the relative contributions of excitatory and inhibitory input to spike variability in the model. Simulations were conducted in which either the gc conductance was constant in the presence of 1 Hz sc input, or the sc conductance was constant in the presence of 30 Hz gc input (Fig. 7D,E). We found that both simulations resulted in a realistic ISI distribution,

but excitatory input variability resulted in a different ISI distribution than inhibitory input variability. In particular, a constant sc conductance with variable gc input resulted in an ISI distribution without a pronounced tail (Fig. 7D). This finding raised two possibilities, namely that long tails in the ISI distribution were a result of the kinetics of inhibitory input or were due to the slow rate of sc input used. To dissociate between these two possibilities, we ran a simulation with 30 Hz sc and 30 Hz gc input and adjusted unitary inhibitory conductances such that the mean level of inhibitory synaptic conductance remained identical. This simulation did not have a tail in the ISI distribution (Fig. 7F), indicating that it was the low frequency of inhibitory input of previous simulations that was responsible for a pronounced tail in the ISI distribution rather than the kinetics of the sc conductance. In addition, we ran simulations, in which we changed the long decay time constant of GABA_A conductance from 26.5 ms in the standard model to 8 ms. When the reduced duration of IPSPs was compensated for by an increase in the peak conductance of single sc synapses, the resulting ISI distributions with a rate of 1Hz sc input did show a pronounced tail. These results lead to the prediction that the tail of Purkinje cell ISI distributions *in vivo* is a result of a relatively low rate of inhibitory inputs.

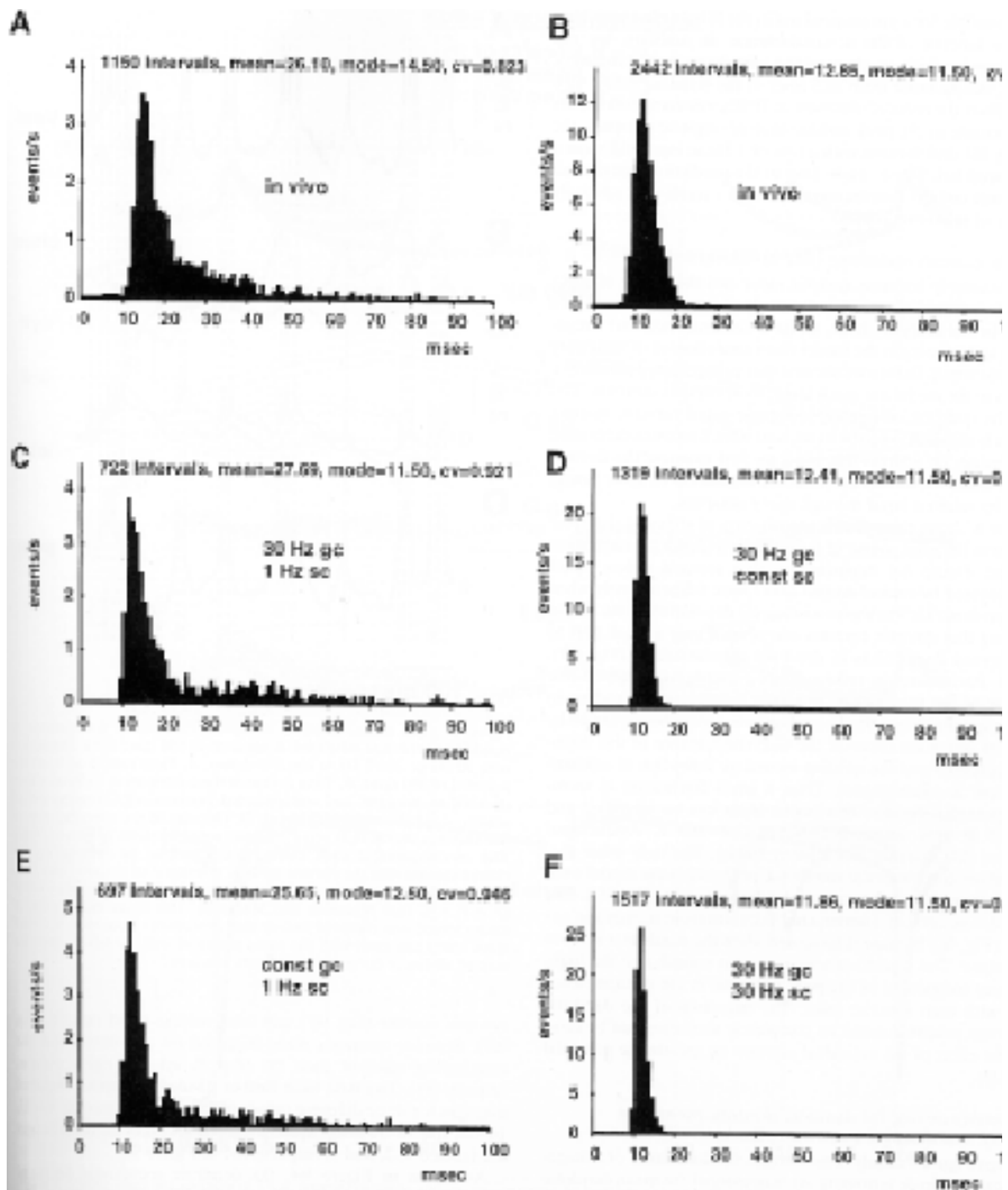


Figure 7

Inter-spike interval distributions for Purkinje cell spike trains.

A,B: Baseline spike rate over 20 s of recording from two Purkinje cells obtained *in vivo* in the anesthetized rat. The mean, mode and coefficient of variation ($cv = \text{standard deviation} / \text{mean}$) of the spike interval distribution are printed above. These recordings presented two typical cases in the range of ISI distributions found in a sample of 15 recorded cells. Typically, the spontaneous spike rate was high and the peak in the ISI distribution around the modal interval was pronounced. The tail of the distribution was frequently larger than expected from an exponential decay. A pronounced tail was associated with a large cv . Values of cv in our sample ranged from 0.3 to 1.4 (mean = 0.7). The small number of very short intervals (< 7 ms) was likely due to spontaneous

climbing fiber input that resulted in a brief burst of 2-3 spikes.

C-F: ISI distributions obtained with different synaptic input rates in simulations of 20 s duration. See Results for description.

Dendritic currents underlying spike variability.

The relationship between synaptic input and the timing of spike output is a central question in the study of neuronal information coding. In our analysis above we have demonstrated that irregularity in spike timing in the model was a consequence of variability in synaptic input. Before we showed that voltage-gated membrane currents in the model are much larger than synaptic currents. This poses the question of how these voltage-gated currents interact with fluctuations in synaptic input, and what processes determine spike timing. To address this issue, we first examine the fluctuations of dendritic membrane currents in relation to spike timing caused by random input through many synapses.

Figure 8 shows the relative contribution of different dendritic currents to the time course of fluctuations in dendritic membrane potential. Figure 8A demonstrates that somatic spikes (spike times denoted by vertical dashed lines) were triggered only when the mean dendritic V_m was in a relatively depolarized state. Surprisingly, synaptic currents contributed only a small part to the observed fluctuations in dendritic depolarization (Fig. 8B). Instead, fluctuations in voltage-gated currents were responsible for most of the increases in dendritic depolarization leading to somatic spiking (Fig. 8B). These fluctuations can be explained by the steep activation curve of the CaP conductance at this membrane potential, and the ensuing secondary activation of calcium-dependent K conductances. Thus, a small fluctuation in membrane potential due to synaptic input can be amplified and changed in time course due to CaP and K conductance dynamics (De Schutter & Bower 1994c). The only other currents influencing dendritic membrane potential in the model were the leak current and the somato-dendritic current (Fig. 8C). The outward leak current counteracted fluctuations in membrane potential (Fig. 8C), as it increased when the dendrite was more depolarized. The somato-dendritic current contributed the high-frequency component of the peak potential in the dendrite associated with each somatic spike. The trajectory of the dendritic membrane potential could be completely reconstructed by summing the effect of the individual currents on membrane potential (Fig. 8D).

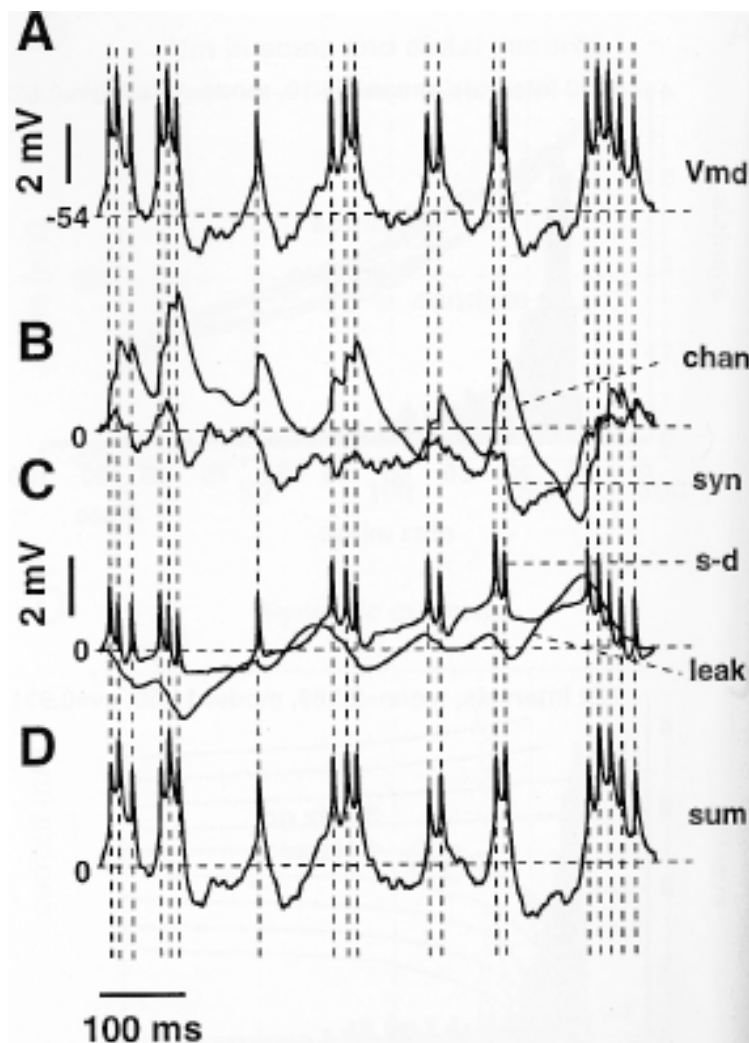


Figure 8

The contribution of individual currents to fluctuations in dendritic membrane potential. A segment of 650 ms for a simulation with 30 Hz gc and 1 Hz sc input is shown.

A: Time course of Vmd for a period of 650 ms.

B: Time course of the contribution to fluctuations in Vmd by synaptic and voltage-gated currents.

C: Contribution of somato-dendritic and leak current.

D: The sum of the contributions of the currents shown in (B) and (C) reconstructed the time course of Vmd. The contribution of each current was obtained by calculating the charge carried with the current (charge is integral of current) and then rescaling the charge to its equivalent change in membrane potential by $Q = V * C$ (see methods). The linear component of each current was removed prior to this procedure. Note that the Vmd trace starts and ends with the same potential, and that therefore the sum of all linear current components was zero.

The relation between ISI duration, dendritic membrane potential, and dendritic current amplitudes.

While Fig. 8 clearly demonstrates the dominance of voltage-gated currents in determining the trajectory of the mean dendritic Vm in the model, it does not directly address the issue of which currents determine the duration of ISIs. To examine how the level of dendritic depolarization and dendritic membrane currents were related to ISI duration in the model we examined

spike triggered averages of these variables for spikes occurring before and after ISIs of different duration (Fig. 9). Spike triggered averages were constructed for the mean voltage level of the dendrite (Fig. 9A), excitatory and inhibitory synaptic conductance (Fig. 9B), total synaptic current (Fig. 9C) and total voltage-gated current (Fig. 9D). Separate averages were triggered on the initial and the terminating spike of each ISI (left and right column in Fig. 9, respectively). The data were further divided into spike triggered averages for three different ranges of ISI duration, namely 10-13 ms, 16-20 ms, and 30-50 ms. Spike triggered averages for these ranges are labeled 1, 2, and 3 respectively in Fig. 9.

As shown in Fig. 9A the dendritic membrane potential (V_{md}) prior to the initial spike of each ISI was on average the same for all three sets of ISI durations. Thus, the initial state of dendritic depolarization was no indication of the subsequent ISI duration for these spike triggered averages.

Immediately following the first spike in an interval, however, the voltage traces for the three sets of ISI duration diverged. The trace in which the terminating spike followed most rapidly (10-13 ms) maintained a more depolarized state after the initial spike than the trace representing 30-50 ms intervals. The depolarization for 16-20 ms intervals was intermediate between the sets of short and long intervals. The 95% confidence limits for the population means of the different sets of intervals show that these differences were highly significant (dashed lines in Fig. 9A). The difference in the level of dendritic depolarization for short and long intervals remained significant until the terminating spike occurred (Fig. 9A, right panel).

The level of sc conductance was well related to ISI duration, whereas the level of gc conductance was not (Fig. 9B). In contrast to V_{md} , the level of sc conductance showed a dependence on ISI duration already before the initial spike of the respective ISI (Fig. 9B). In particular, the net sc conductance in the 5 ms preceding an ISI was significantly larger before an ISI of 30-50 ms duration than before a 10-13 ms ISI. This difference in sc conductance for ISIs of different duration increased in the first 10 ms following the initial spike and decayed gradually before the terminating spike of the respective ISI. Therefore, a strong effect of inhibitory input on ISI duration occurred early during the ISI. In contrast, the gc conductance showed no difference for ISIs of different durations.

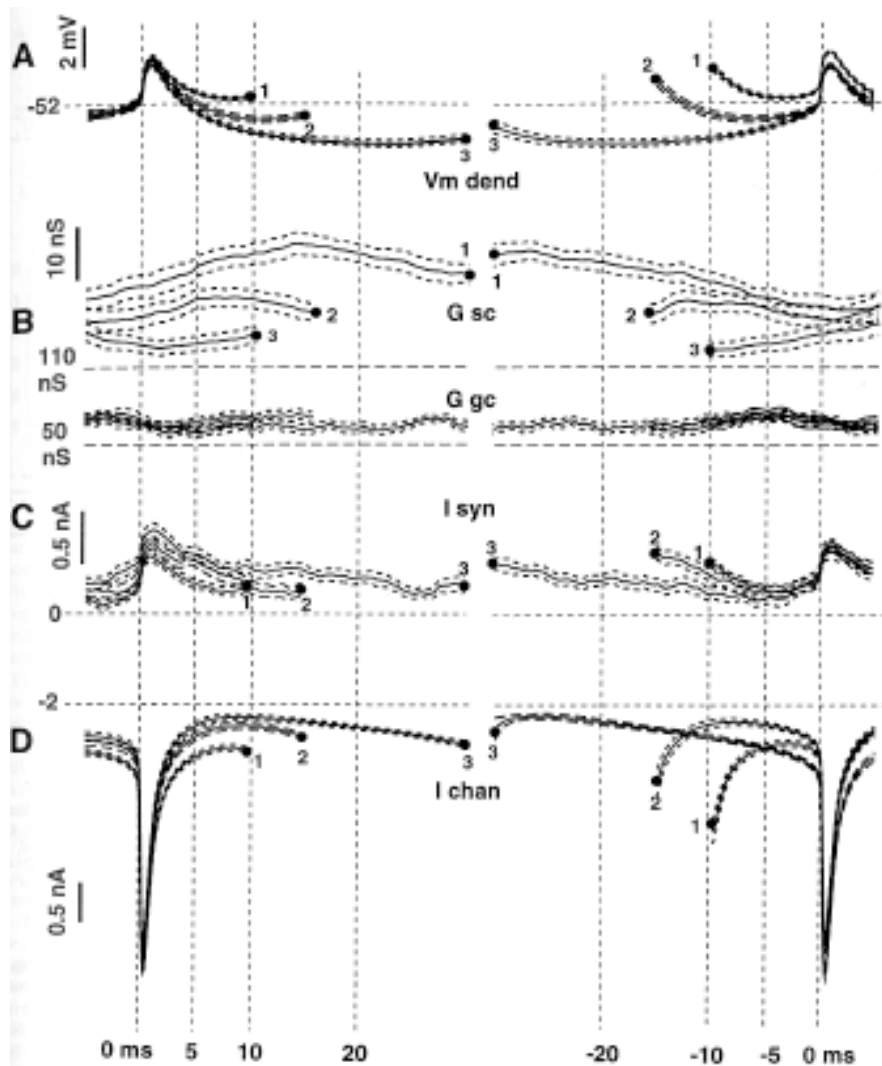


Figure 9

Spike-triggered averages of Vmd, synaptic currents, and channel currents. Spike-triggered averages were constructed for 3 sets of ISIs from 7 s of simulation with 30 Hz gc and 1 Hz sc input. The ISI distribution for this level of input is shown in Fig. 7C. Set 1 included 74 ISIs of 10-13 ms, set 2 included 32 ISIs of 16-20 ms, and set 3 included 39 ISIs of 30-50 ms. An upper and lower 95% confidence limit (1.7 standard errors) is shown for each spike triggered average as a pair of dashed traces. Vertical dashed lines denote the timing of dendritic traces with respect to the peak depolarization in the soma with each spike. Traces in the left column are aligned to the initial spike in each ISI, and traces on the right are aligned to the terminating spike.

A: Spike-triggered average of Vmd.

B: Spike-triggered average of synaptic conductances summed for all gc inputs (Ggc) and all sc inputs (Gsc) in Siemens * $10e^{-9}$. Note that the total sc conductance is more than twice the amplitude of the gc conductance.

C: Spike-triggered average of summed gc and sc currents (I syn). Note that the peak in synaptic current with each somatic spike is not due to synaptic input but to the change in driving forces for gc and sc conductances with spike-related dendritic depolarization.

D: Spike-triggered average of summed Ca and K currents (I chan). The inward peak of current following each somatic spike is due to the activation of CaP conductance with spike-related dendritic depolarization.

The total synaptic current for the three sets of ISIs reflected the increase in sc conductance in that it was significantly more outward for the set of long ISIs than the set of short ISIs. The increase in current was less pronounced than the increase in conductance, however, since the driving force was reduced at the less depolarized V_m associated with long ISIs. The charge carried by the increased outward synaptic current for long ISIs in the period between 5 ms before and 10 ms after the initial spike accounted for a decrease in dendritic depolarization of 0.87 mV.

Fig. 9D shows that the net inward level of voltage-gated dendritic currents was significantly decreased for long ISIs. As with synaptic current, this difference started before the first spike in the respective ISI. The amplitude of the mean difference for voltage-gated currents between short and long ISIs for consecutive windows of 5 ms duration starting at 5 ms before the first spike was 0.24 nA, 0.39 nA, and 0.4 nA, respectively. Overall, the decrease in inward voltage-gated current with long ISIs accounted for 1.2 mV of dendritic hyperpolarization over 15 ms. Voltage-gated current therefore contributed more to the relative dendritic hyperpolarization seen with long ISIs than did synaptic currents. Interestingly, the influence of voltage-gated currents was reversed just prior to the terminating spike of an ISI (right panel in Fig. 9D). In effect, the increase in inward voltage-gated current before the terminating spike of a long ISI contributed to the depolarization of the dendrite necessary to trigger a somatic spike. This time course again indicates that the dendritic currents around the onset of an ISI determines its length in the case of random input through many synapses.

Somatic currents controlling the timing of individual spikes.

Ultimately the timing of somatic sodium spikes is dependent on the control of NaF activation in the soma. As we showed in Fig. 3, spontaneous somatic spiking in the absence of synaptic input was the result of a dynamic push and pull operation between the soma and the dendrite. In Fig. 10 we examine this process in the presence of synaptic input for single examples of a short and of a long ISI. As in the case without synaptic input, we find that spike after-hyperpolarization is overcome through a current boost from the dendrite, which remains depolarized throughout the spike cycle. For the short ISI (Fig. 10A), this current boost depolarizes the soma sufficiently to lead to a monotonically increasing activation of the NaF current, which directly results in a second spike. In contrast, for the long interval (Fig. 10B), the NaF current is activated less strongly during the current boost from the dendrite, and a tug of war between the subsequent outward current into the dendrite and the inward NaF current ensues. A second spike is generated only when the NaF current escapes the dendritic current sink.

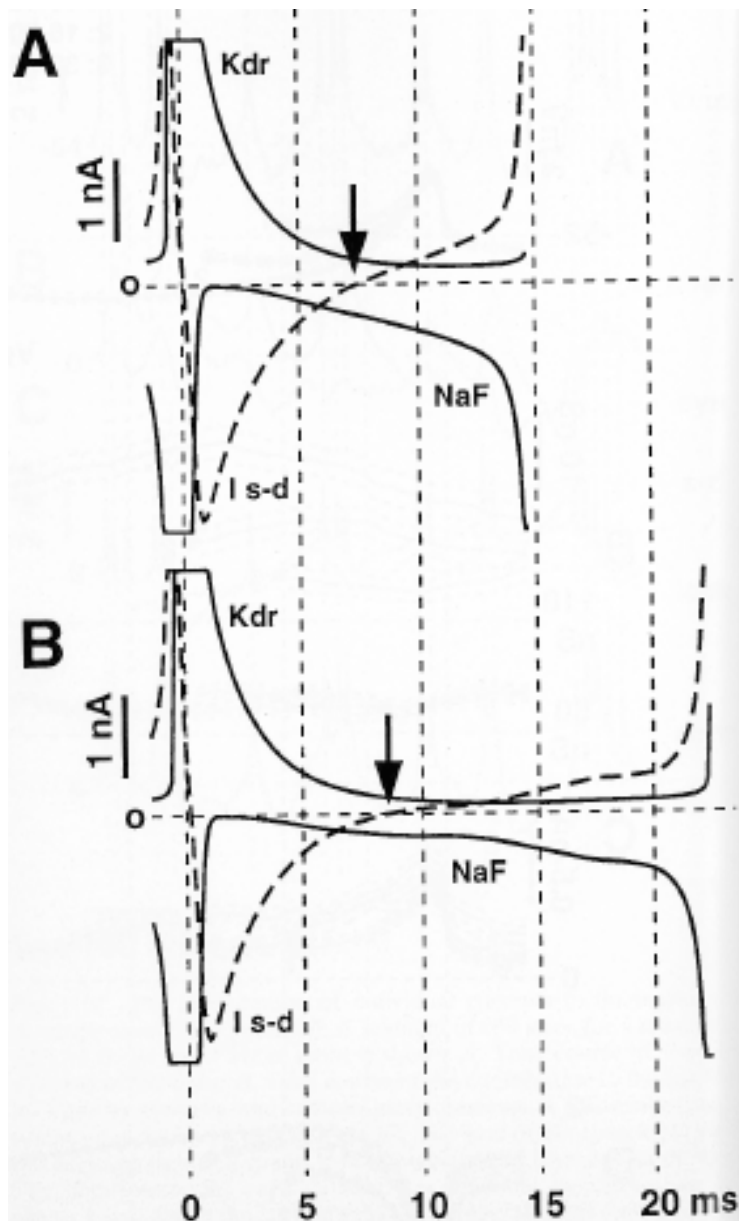


Figure 10

A: Somatic currents during a 15 ms ISI.

B: Same currents during a 23 ms ISI. The black arrows denote the time at which the current from the dendrite into the soma (*I*_{s-d}) reversed, turning the dendrite from a current source into a current sink. As described in the text, the amplitude of the NaF current around the time of *I*_{s-d} reversal was critical for obtaining a short or long ISI. Figure 10 suggests that the state of the somatic NaF current at the time when the phasic boost of current from the dendrite ends (*I*_{s-d} reversal, denoted by black arrows in Fig. 10) may be important in determining ISI duration. This idea is examined more closely in Fig. 11A, which shows a scatter plot of the NaF current at the time of *I*_{s-d} reversal for 261 ISIs of varying duration. In fact, for intervals shorter than 20 ms the amplitude of NaF at *I*_{s-d} reversal showed a high degree of correlation with ISI duration ($r_2 = 71\%$). For longer intervals this correlation broke down, suggesting that events subsequent to *I*_{s-d} reversal determined the precise duration of long intervals. Since the current flow from the dendrite into the soma is

proportional to the voltage difference between the two compartments, it seemed likely that the level of dendritic depolarization at the time of Isd reversal might be an important factor in controlling NaF activation. As we saw above in Fig. 9A, dendritic depolarization was significantly different for short than for long ISIs at the time of somatic spike after-hyperpolarization. Figure 11B shows that the activation of NaF at the time of Isd reversal was indeed highly correlated ($r_2 = 80\%$) with the level of dendritic depolarization at this time. This correlation indicates that somatic re-depolarization following the initial spike of an ISI was under tight control of dendritic depolarization and that NaF was largely activated as a function of this process. Given that the level of NaF activation at the time of Isd reversal correlated well with V_{md} , it is not surprising that V_{md} showed a similar correlation to ISI duration at this time point as did NaF (Fig. 11C). This result extends the observation that V_{md} determines spike timing obtained from spike-triggered averaging to the level of single ISIs (Fig. 9A). As we saw in Fig. 8, dendritic depolarization was controlled more by voltage-gated current than by synaptic current. In fact, we failed to find any significant correlation between the amplitude of excitatory synaptic conductance at any point in time during an ISI and the duration of ISIs. The level of inhibitory conductance at the time of Isd reversal on the other hand did show a significant correlation with ISI duration (Fig. 11D, $r_2 = 24\%$ for ISIs shorter than 20 ms). Nevertheless, this correlation was much weaker than the correlation of V_{md} itself with ISI duration, supporting the findings above that intrinsic properties of the cell have a large influence on ISI duration. In distinction to NaF and V_{md} , the level of sc conductance showed also a small but significant correlation with the duration of long ISIs ($r_2 = 14\%$), suggesting that the duration of long ISIs was partly predetermined at the early time of Isd reversal via the level of inhibition. The precise events that led to the termination of long ISIs were not examined.

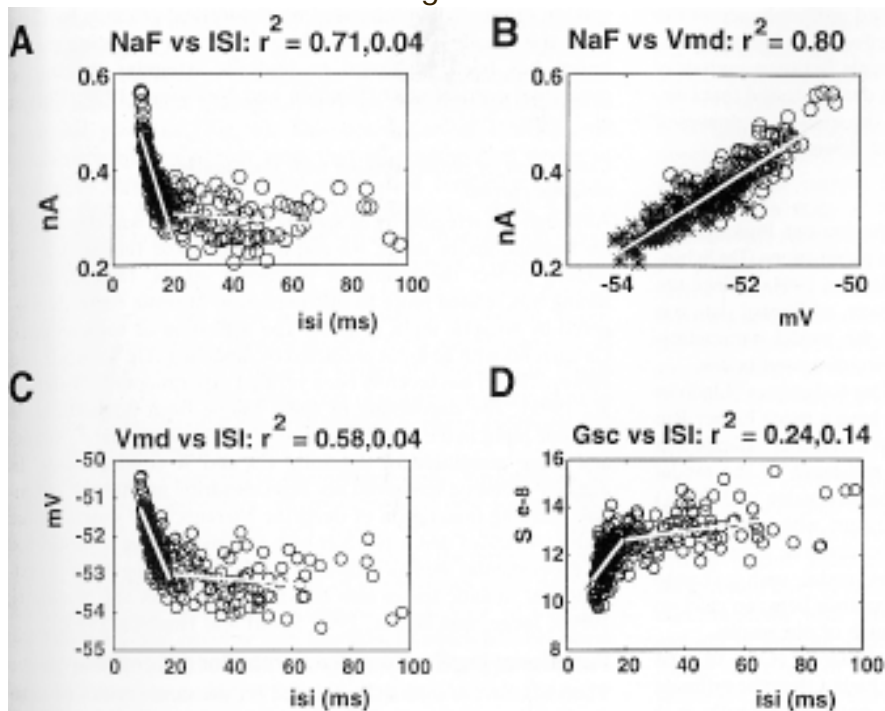


Figure 11

Scatter plots relating current levels and dendritic depolarization at the time of Is-d reversal to ISI duration. Each circle denotes the values for a single ISI out of 7s of simulated data for 30 Hz gc and 1 Hz sc input. Since short intervals (< 20 ms) generally had a higher degree of correlation with different variables at the time of Is-d reversal, two linear regressions were calculated for short and long ISIs, respectively. The correlation coefficients (r_2) for short and long ISIs are printed above each plot.

A: Activation of NaF at the time of Is-d reversal vs. ISI duration.

B: NaF activation vs. Vmd. Values associated with short ISIs (< 20 ms) are denoted by circles, values for long ISIs are denoted by asterisks.

C: Vmd at the time of Is-d reversal vs. ISI duration. **D:** Total sc conductances at the time of Is-d reversal vs. ISI duration.

Overall, the relatively small control of synaptic input over the timing of somatic spikes was shown multiple times in the preceding analyses. This result ensued from dendritic voltage-gated conductances, which caused a strong indirection in the influence of synaptic input on spike timing. As discussed below, these findings have important implications for neuronal coding by Purkinje cells in the cerebellar cortical network.

Discussion

We examined in a realistic Purkinje cell model how intrinsic currents interact with synaptic input to control somatic spiking. Although we supported model behavior with physiological data, the validity of any modeling results depends on the choice of model parameters and analysis procedures. We will first discuss our modeling assumptions. We will then consider the significance of the present results with respect to the input-output function of the Purkinje cell and implications for cerebellar function. Finally, we will propose several experimentally testable predictions based on our analysis.

Validity of modeling results

Limitations due to disregarding spatial aspects of dendritic function.

While summing currents across the whole dendritic tree reduced the complexity of our analysis significantly, this technique neglects all spatial aspects of dendritic processing. Several factors mitigate this problem in the present study. First, dendritic conductances were distributed uniformly in the model, thus avoiding spatially restricted modes in current activation. Recent calcium imaging studies support the concept of uniformly distributed conductances in the Purkinje cell dendrite (Lev-Ram, Miyakawa, et al. 1992). Second, synaptic input was also distributed uniformly across the dendrite with no attempt to examine the effect of clustered inputs, or to generate special spatial arrangements between excitatory and inhibitory inputs. A previous analysis demonstrated that clustering inputs did not substantially change the somatic responses of the Purkinje cell model (De Schutter & Bower 1994c). While the spatial arrangement of synaptic inputs to Purkinje cells may have a significant effect on dendritic processing, there is at present no information on the spatial or temporal patterns of synaptic input *in vivo* that could be used to constrain inputs in the model.

Accuracy in model properties.

Any computer model can only present an approximation to the properties of a biological neuron. The data and assumptions relating to the present Purkinje cell model were discussed in detail in previous publications (De Schutter & Bower 1994a; De Schutter & Bower 1994a). Since the original construction of this model, however, additional data has become available related to several of the model's parameters. Their significance for the present study are discussed below.

Recent studies using whole cell recording techniques (Llano, Marty, et al. 1991) have shown that Purkinje cells have a much higher R_m than previously demonstrated with sharp electrodes (Llinás & Sugimori 1980a). Increasing the input resistance of the model from the present value of 19.6 M Ω to the new value of 160 M Ω would considerably reduce the leakage current, with less compensating Ca current necessary to keep the dendrite depolarized. While reducing the Ca current in the model, such a change would not affect the voltage-dependent balance between calcium and potassium currents that underlies much of our results.

The value of specific membrane capacitance (C_m) of 1.64 $\mu\text{F} / \text{cm}_2$ used in the model is considerably higher than the estimate of C_m of 0.8 $\mu\text{F} / \text{cm}_2$, which has recently been obtained in a careful study of hippocampal pyramidal cells (Major, Larkman, et al. 1994). Lowering C_m to 0.8 $\mu\text{F} / \text{cm}_2$ in the model would half the charge needed to change membrane potential by a given amount. Like an increase in R_m , reducing C_m would lead to a reduction in the overall amplitude of intrinsic currents, but would not affect the voltage-dependent interaction between individual currents.

Control of spiking in the Purkinje cell model

The general question of what information about synaptic input is coded in spike has recently received a lot of attention (Shadlen & Newsome 1994; Mainen & Sejnowski 1995; Softky 1995; Powers & Binder 1996; König, Engel, et al. 1996). The present study allows us to address this issue for the cerebellar Purkinje cell.

Irregularity of spiking with a large number of background inputs.

Softky and Koch (1993) argued, based on the law of large numbers, that cells receiving many randomly firing excitatory synapses should produce a highly regular output spike train. As shown in Fig. 7, Purkinje cell spike trains *in vivo* are highly irregular in spite of the fact that Purkinje cells have a very large number of excitatory synapses (175,000 in rats, xxx(Napper & Harvey 1988b), which have an estimated baseline activity of 0.3 Hz each (Huang, Mu, et al. 1993). Usher et al. (1994) in analyzing cerebral cortical networks suggested that irregular firing could be a result of local excitatory feedback within cortex. This solution cannot apply to Purkinje cell spiking, however, as the cerebellar cortex completely lacks excitatory feedback connections. Our findings suggest that the irregularity of Purkinje cell spiking is due to an overall balance between inward and outward currents keeping the cell close to firing threshold (Fig. 5). This balance allows small fluctuations in synaptic input to influence spike timing, since a summation of excitatory inputs to drive the cell to threshold is unnecessary. The

mechanism we describe is similar to a random walk model of irregular spiking originally hypothesized on theoretical grounds by Gerstein and Mandelbrot (1964). More recently a balancing mechanism has been suggested to underlie irregular spiking in pyramidal cortical cells (Shadlen & Newsome 1994; Bell, Mainen, et al. 1996), but firm experimental support is lacking. The present report is the first demonstration of such a mechanism in a model closely tied to experimental data.

The correlation of output spiking with fluctuations in synaptic current.

Although the irregularity of spiking in the model was dependent on fluctuations in input, we showed that spike timing did not directly reflect the timing of preceding inputs. Instead, spike timing was more related to fluctuations in intrinsic currents triggered by synaptic input (Fig. 8). The activation of voltage-gated Ca currents with granule cell input predicted by modeling (De Schutter & Bower 1994c) has recently been verified experimentally (Eilers, Augustine, et al. 1995). The decoupling of spike timing from fluctuations in synaptic input in the model was a result of the long time constants and large amplitude of dendritic Ca and K conductances. In addition, somatic spikes did not reset dendritic membrane potential, allowing integration of dendritic currents over several spike cycles. A lack of dendritic reset with somatic spiking is supported by experimental studies showing rapidly attenuating back propagation of somatic spikes into the dendrite (Linás & Sugimori 1980b; Jaeger & Bower 1994; Stuart & Hausser 1994).

Functional implications for cerebellar processing

Theorists have traditionally focused on the nearly crystalline anatomical layout of cerebellar cortex to construct models of cerebellar function (Marr 1969; Albus 1971; Kanerva 1988; Braitenberg 1993). The biophysical properties of single cells have been largely neglected in these theories, and Purkinje cells are treated as simple summation devices. Important implications for network function based on the more complex Purkinje cell properties we find are discussed below.

A central role for inhibitory input.

In the model, the presence of a baseline of outward synaptic current through inhibitory synapses was essential to control the depolarization due to the large intrinsic calcium current. Without inhibition the Purkinje cell dendrite will progressively depolarize and generate spontaneous calcium spikes both in the model (De Schutter & Bower 1994b) and *in vivo* (Jaeger & Bower 1994). Such spontaneous calcium spikes are not seen normally *in vivo* (Jaeger & Bower 1994). The intrinsic activation of voltage-gated currents underlying this depolarization is supported by results showing that this behavior persists after excitatory synaptic transmission is blocked *in vitro* (Jaeger, unpublished results).

Spike timing was also much more sensitive to rapid changes in inhibitory inputs than in excitatory inputs (Figs. 9B and 11D). The essential role of inhibition in determining spike rate and timing has not been recognized in established theories of cerebellar cortical function (Marr 1969; Albus 1971). Instead, in these models stellate cell input is largely treated as providing

surround inhibition to foci or beams of activation. Our results suggest that the geometry and precise time course of the activation of stellate cells by granule cells is very important and should be examined in future physiological studies.

Functionality of the Purkinje cell in the cerebellar network.

Our modeling results indicate that the baseline level of open excitatory and inhibitory synaptic conductances exerted a partial voltage clamp on the dendrite, and that actual dendritic membrane potential stayed close to the clamping voltage determined by the reversal potentials of the synaptic conductances. As a consequence, changes in the activity of any set of synaptic inputs were effective in changing the membrane potential and hence spike rate. In fact, the soma was very sensitive to small changes in dendritic depolarization (Fig. 6). This description of Purkinje cell behavior is quite different from that commonly made in theories of cerebellar cortex. In particular, most established theories (Marr 1969; Albus 1971; Fujita 1982; Kanerva 1988) regard the Purkinje cell as a summation device. In such an integrate-and-fire formalism, sensitivity to small numbers of input in the presence of a high baseline of inputs is lost. These theories accommodate this problem by assuming that only a small number of input synapses are active or have a significant weight. If our predictions are correct, small changes in synaptic input in the presence of a large baseline may be significant for spiking. De Schutter (1995) has proposed that changes in synaptic weight may function to maintain the balance between excitation and inhibition over long time.

A consequence of the large contribution of intrinsic currents to dendritic depolarization in the model was that the exact timing of somatic spikes did not reflect preceding inputs directly. This poses a problem for theories that assume that the timing of Purkinje cell spikes accurately reflects the timing of parallel fiber inputs (Braitenberg & Atwood 1958). Instead, Bower (1996) has recently proposed a new view of how cerebellar cortical circuitry may function, in which the indirect modulation of spiking by parallel fiber input is incorporated. While not examined in the present study, the balance of parallel fiber and stellate cell inputs could modulate the response of the Purkinje cell to a more synchronous and exclusively excitatory input expected to occur via the ascending branch of the granule cell axon (Bower, 1996). Previous modeling results have suggested that such a synchronous granule cell input can produce a timelocked somatic spike (De Schutter 1994).

Model-based experiments and predictions.

The present analysis identifies several model parameters that are critical for the described behavior. The results also lead to specific predictions about the role of synaptic input in controlling Purkinje cell spiking. Due to the direct correspondence between data traces generated by the model and physiological traces, we can propose specific experiments that test the validity of critical model assumptions as well as our functional predictions.

Voltage gated membrane currents.

The P-type calcium channel provided a crucial current in the model that kept

the dendrite depolarized, and that was strongly modulated with changes in synaptic input. Experimental findings support the presence of sustained dendritic plateau depolarizations due to the CaP conductance (Llinás & Sugimori 1980b; Llinás & Sugimori 1992) and the kinetics of CaP are well established (Regan 1991; Usowicz, Sugimori, et al. 1992). Our results with respect to the exact amplitude of this current, the time course of activation with synaptic input, and the secondary activation of Ca-dependent K conductances need experimental verification, however. Possible experiments involve the use of dynamic current clamping (Sharp, O'Neil, et al. 1993; Robinson & Kawai 1993). Using this approach an experimentalist can apply artificial synaptic conductances to a neuron recorded *in vitro*. Specific CaP blockers (Adams, Mintz, et al. 1993) can be used to examine the involvement of this current in responses to such controlled input. We would predict that total blockage of CaP results in dendritic hyperpolarization as well as a shortening and decreased amplitude in the response to excitatory synaptic conductances.

The somatic subthreshold Na current was also very important in the model, as it greatly influenced the interaction between dendritic depolarization and somatic spiking (Fig. 11). Subthreshold Na currents have been demonstrated in somatic recordings *in vitro* (Llinás & Sugimori 1980a; Llinás & Sugimori 1992). It is not clear at present whether this subthreshold current is due to a Na window current (De Schutter & Bower 1994a), to a distinct open state of the fast Na conductance (Gähwiler & Llano 1989; Alzheimer, Schwindt, et al. 1993), or partly carried by a different persistent Na conductance (Sugimori, Kay, et al. 1994). Any of these currents are likely to be deactivated during the spike after-hyperpolarization seen in Purkinje cell recordings (Llinás & Sugimori 1980a; Jaeger & Bower 1994). Our predicted pattern of current flow during a somatic spike cycle is open to direct experimental verification. The crucial experiment would measure the membrane potential in the soma and in the main dendrite simultaneously to determine the direction and amplitude of current flow at different times.

Synaptic inputs.

There is little information available on the activity pattern of synaptic inputs impinging on a Purkinje cell *in vivo*. As a result, the values used in the model for these parameters are best-guess estimates (De Schutter & Bower 1994b). The present study predicts a considerable voltage clamping effect of baseline synaptic conductances such that any disturbance in membrane potential is counteracted by changing synaptic driving forces. The strength of this effect and therefore the background level of synaptic conductances *in vivo* can be assessed experimentally with intracellular recordings. For example, the amount of synaptic clamping current can be examined by comparing the effect of current injection before and after synaptic inputs are pharmacologically blocked. The difference in effect of a given current amplitude on membrane potential is directly related to the amount of clamping current provided by baseline synaptic conductances.

Rate coding of synaptic input levels.

In addition to suggesting experiments relevant to model parameters, it is

important to identify experiments that could test the overall conclusions. One of our most striking findings was that the timing of individual spikes did not faithfully reflect synaptic input fluctuations, but the mean spike rate showed a high gain function for the balance between excitatory and inhibitory inputs (Fig. 6). These predictions can be verified experimentally with the technique of dynamic current clamping mentioned above. We would predict that a baseline of open excitatory and inhibitory conductances will result in a synaptic current with near-zero amplitude with any spike rate up to 100 Hz, and that the combined reversal potential of the synaptic conductances will determine this spike rate. Furthermore, the recorded membrane potential and individual spike times under these conditions should not directly reflect the waveform of applied synaptic conductances, but should depend largely on voltage-gated currents as predicted by the model.

References

- Agmon-Snir H, Segev I (1993) Signal delay and input synchronization in passive dendritic structures. *J Neurophysiol* 70:2066-2085.
- Albus JS (1971) A theory of cerebellar function. *Math Biosci* 10:25-61.
- Alzheimer C, Schwindt PC, Crill WE (1993) Modal gating of Na⁺ channels as a mechanism of persistent Na⁺ current in pyramidal neurons from rat and cat sensorimotor cortex. *J Neurosci* 13:660-673.
- Barbour B (1993) Synaptic currents evoked in Purkinje cells by stimulating individual granule cells. *Neuron* 11:759-769.
- Bell A, Mainen ZF, Tsodyks M, Sejnowski TJ. (1995) Balancing of conductances may explain irregular cortical spiking. Tech Report #INC-9502, Salk Institute, San Diego
- Bower JM, Kassel J (1990) Variability in tactile projection patterns to cerebellar folia Crus IIA of the Norway rat. *J Comp Neurol* 302:768-778.
- Bower JM, Woolston DC (1983) Congruence of spatial organization of tactile projections to granule cell and Purkinje cell layers of cerebellar hemispheres of the albino rat: Vertical organization of cerebellar cortex. *J Neurophysiol* 49:745-766.
- Braitenberg V, Atwood RP (1958) Morphological observations on the cerebellar cortex. *J Comp Neurol* 109:1-33.
- Buonomano DV, Merzenich MM (1995) Temporal information transformed into a spatial code by a neural network with realistic properties *Science* 267:1028-1030.
- [De Schutter E](#) (1994) Modelling the cerebellar Purkinje cell: experiments in computo. In: *Progress in Brain Research* Vol. 102 (van Pelt, J.; Corner, M. A.; Uylings, H. B. M.; Lopes da Silva, F. H.). pp 427-441. Elsevier.
- [De Schutter E](#) (1995) Cerebellar long-term depression might normalize excitation of Purkinje cells. *Trends Neurosci* 18:291-295.
- [De Schutter E, Bower JM](#) (1994a) An active membrane model of the cerebellar Purkinje cell I. Simulation of current clamp in slice. *J Neurophysiol* 71:375-400.
- [De Schutter E, Bower JM](#) (1994b) An active membrane model of the cerebellar Purkinje cell II. Simulation of synaptic responses. *J Neurophysiol*

71:401-419.

[De Schutter E, Bower JM](#) (1994c) Simulated responses of cerebellar Purkinje cells are independent of the dendritic location of granule cell synaptic inputs. *Proc Natl Acad Sci USA* 91:4736-4740.

Eccles JC, Llinás R, Sasaki K (1966) Parallel fibre stimulation and the responses induced thereby in the Purkinje cells of the cerebellum. *Exp Brain Res* 1:17-29

Gšhwiler BH, Llano I (1989) Sodium and potassium conductances in somatic membranes of rat Purkinje cells from organotypic cerebellar cultures. *J Physiol (Lond)* 417:105-122.

Gruol DL, Dionne VE, Yool AJ (1989) Multiple voltage-sensitive K⁺ channels regulate dendritic excitability in cerebellar Purkinje neurons. *Neurosci Lett* 97:97-102.

Gruol DL, Jacquin T, Yool AJ (1991) Single-channel K⁺ currents recorded from the somatic and dendritic regions of cerebellar Purkinje neurons in culture. *J Neurosci* 11:1002-1015.

Harris NC, Ramsay S, Kelion A, Greenfield SA (1989) Electrophysiological evidence for the dendritic localization of a calcium conductance in guinea-pig substantia nigra neurones in vitro. *Exp Brain Res* 74:411-416.

Harvey RJ, Napper RMA (1991) Quantitative studies of the mammalian cerebellum. *Prog Neurobiol* 36:437-463.

Hopfield JJ, Herz AVM (1995) Rapid local synchronization of action potentials: Toward computation with coupled integrate-and-fire neurons. *Proc Natl Acad Sci USA* 92:6655-6662.

Huang CM, Mu H, Hsiao CF (1993) Identification of cell types from action potential waveforms: cerebellar granule cells. *Brain Res* 619:313-318.

Jaeger D, Bower JM (1994) Prolonged responses in rat cerebellar Purkinje cells following activation of the granule cell layer: an intracellular in vitro and in vivo investigation. *Exp Brain Res* 100:200-214.

Kandel ER; Schwartz JH; Jessell TM (1991) *Principles of Neural Science*. New York: Elsevier.

Karst H, Joels M, Wadman WJ (1993) Low-threshold calcium current in dendrites of the adult rat hippocampus. *Neurosci Lett* 164:154-158.

Kim HG, Connors BW (1993) Apical dendrites of the neocortex: correlation between sodium- and calcium-dependent spiking and pyramidal cell morphology. *J Neurosci* 13:5301-5311.

Koch C, Bernander O, Douglas RJ (1995) Do neurons have a voltage or a current threshold for action potential initiation? *J comp Neurosci*. 2:63-82.

Lev-Ram V, Miyakawa H, Lasser-Ross N, Ross WN (1992) Calcium transients in cerebellar Purkinje neurons evoked by intracellular stimulation *J Neurophysiol* 68:1167-1177.

Lev-Tov A, Miller JP, Burke RE, Rall W (1983) Factors that control amplitude of EPSPs in dendritic neurons. *J Neurophysiol* 50:399-412.

Llano I, Marty A, Armstrong CM, Konnerth A (1991) Synaptic- and agonist-induced excitatory currents of Purkinje cells in rat cerebellar slices. *J Physiol (Lond)* 434:183-213.

Llinás R, Sugimori M (1980a) Electrophysiological properties of in vitro

Purkinje cell somata in mammalian cerebellar slices. *Physiol (Lond)* 305:171-195.

Llinás R, Sugimori M (1980b) Electrophysiological properties of in vitro Purkinje cell dendrites in mammalian cerebellar slices. *J Physiol (Lond)* 305:197-213.

Llinás R; Sugimori M (1992) The electrophysiology of the cerebellar Purkinje cell revisited. In: *The Cerebellum Revisited* (Llinás, R.; Sotelo, C.). pp 167-181. New York: Springer Verlag.

Lytton WW, Sejnowski TJ (1991) Simulations of cortical pyramidal neurons synchronized by inhibitory interneurons. *J Neurophysiol* 66:1059-1079.

Magee JC, Johnston D (1995) Synaptic activation of voltage-gated channels in the dendrites of hippocampal pyramidal neurones. *Science* 268:301-304.

Major G, Larkman AU, Jonas P, Sakmann B, Jack JJB (1994) Detailed passive cable models of whole-cell recorded CA3 pyramidal neurons in rat hippocampal slices. *J Neurosci* 14:4613-4638.

Markram H, Sakmann B (1994) Calcium transients in dendrites of neocortical neurons evoked by single subthreshold excitatory postsynaptic potentials via low-voltage-activated calcium channels. *Proc Natl Acad Sci USA*. 91:5207-5211.

Marr D (1969) A theory of cerebellar cortex. *J Physiol (Lond)* 202:437-471.

Mel B (1993) Synaptic integration in an excitable dendritic tree. *J Neurophysiol* 70:1086-1101.

Miller JP, Rall W, Rinzel J (1985) Synaptic amplification by active membrane in dendritic spines. *Brain Res* 325:325-330.

Murphy JT, Sabah NH (1971) Cerebellar Purkinje cell responses to afferent inputs. II. Mossy fiber activation. *Brain Res* 25:469-482.

Napper RMA, Harvey RJ (1988b) Number of parallel fiber synapses on an individual Purkinje cell in the cerebellum of the rat. *J Comp Neurol* 274:168-177.

Nedergaard S, Bolam JP, Greenfield SA (1988) Facilitation of a dendritic calcium conductance by 5-hydroxytryptamine in the substantia nigra. *Nature* 333:174-177.

Palay SL, Chan-Palay V. (1974). *Cerebellar Cortex*. New York: Springer-Verlag.

Rall W, Burke RE, Smith TRG, Nelson PG, Frank K (1967) Dendritic location of synapses and possible mechanisms for the monosynaptic EPSP in motoneurons. *J Neurophysiol* 30:1169-1193.

Rapp M, Segev I, Yarom Y (1994) Physiology, morphology and detailed passive models of guinea-pig cerebellar Purkinje cells. *J Physiol (Lond)* 474:101-118.

Rapp M, Yarom Y, Segev I (1992) The impact of parallel fiber background activity on the cable properties of cerebellar Purkinje cells. *Neural Comput* 4:518-533.

Regan LJ (1991) Voltage-dependent calcium currents in Purkinje cells from rat cerebellar vermis. *J Neurosci* 11:2259-2269.

Regehr WG, Tank DW (1992) Calcium concentration dynamics produced by synaptic activation of CA1 hippocampal pyramidal cells. *J Neurosci*

12:4202-4223.

Segev I, Rall W (1988) Computational study of an excitable dendritic spine. *J Neurophysiol* 60:499-523.

Softky W (1994) Sub-millisecond coincidence detection in active dendritic trees. *Neuroscience* 58:13-41.

Softky WR, Koch C (1993) The highly irregular firing of cortical cells is inconsistent with temporal integration of random EPSPs. *J Neurosci* 13:334-350.

Staub C, De Schutter E, Knöpfel T (1994) Voltage-imaging and simulation of effects of voltage- and agonist activated conductances on soma-dendritic voltage coupling in cerebellar Purkinje cells. *J comp Neurosci* 1:301-311.

Stuart G, Häusser M (1994) Initiation and spread of sodium action potentials in cerebellar Purkinje cells. *Neuron* 13:703-712.

Sugimori M, Kay AR, Llinás R (1994) The persistent Na⁺ current in cerebellar Purkinje cells has a single channel conductance distinct from the inactivating current. *Soc Neurosci Abstr* 20, part 1:63.

Sugimori M, Llinás R (1992) Dual patch-clamping of mammalian Purkinje cells in cerebellar slices. *Soc Neurosci Abstr* 18, Part 2:1358-1358.

Usher M, Stemmler M, Koch C, Olami Z (1994) Network amplification of local fluctuations causes high spike rate variability, fractal firing patterns and oscillatory local field potentials. *Neural Comp* 6:795-836.

Usovich MM, Sugimori M, Cherksey B, Llinás R (1992) P-type calcium channels in the somata and dendrites of adult cerebellar Purkinje cells. *Neuron* 9:1185-1199.

Vincent P, Armstrong CM, Marty A (1992) Inhibitory synaptic currents in rat cerebellar Purkinje cells: Modulation by postsynaptic depolarizations. *J Physiol (Lond)* 456:453-471.

Yuste R, Gutnick MJ, Saar D, Delaney KR, Tank DW (1994) Ca²⁺ accumulations in dendrites of neocortical pyramidal neurons: an apical band and evidence for two functional compartments. *Neuron* 13:23-43.

[Download the model scripts.](#)